

Testing Large-Scale Structure Measurements Against Fisher Matrix Predictions

Setareh Foroozan^{a,b} Alex Krolewski^{a,b,c} Will J. Percival^{a,b,c}

^aWaterloo Centre for Astrophysics, University of Waterloo, 200 University Ave W, Waterloo, ON N2L 3G1, Canada

^bDepartment of Physics and Astronomy, University of Waterloo, 200 University Ave W, Waterloo, ON N2L 3G1, Canada

^cPerimeter Institute for Theoretical Physics, 31 Caroline St. North, Waterloo, ON N2L 2Y5, Canada

E-mail: s2forooz@uwaterloo.ca

Abstract. We compare Baryonic Acoustic Oscillation (BAO) and Redshift Space Distortion (RSD) measurements from recent galaxy surveys with their Fisher matrix based predictions. Measurements of the position of the BAO signal lead to constraints on the comoving angular diameter distance D_M and the Hubble distance D_H that agree well with their Fisher matrix based expectations. However, RSD-based measurements of the growth rate $f\sigma_8$ do not agree with the predictions made before the surveys were undertaken, even when repeating those predictions using the actual survey parameters. We show that this is due to a combination of effects including degeneracies with the geometric parameters D_M and D_H , and optimistic assumptions about the scale to which the linear signal can be extracted. We show that measurements using current data and large-scale modelling techniques extract an equivalent amount of signal to that in the linear regime for $k \lesssim 0.08 h \text{ Mpc}^{-1}$, remarkably independent of the sample properties and redshifts covered.

Contents

1	Introduction	1
2	Methodology	2
2.1	The Fisher matrix for the BAO measurements	3
2.2	The Fisher matrix for the RSD measurements	4
2.3	Integration Limits (k_{\min} and k_{\max})	5
3	Data and modelling	6
3.1	Reconstruction Technique	6
3.2	RSD modelling	7
3.3	6-degree Field Galaxy Survey	8
3.4	Main Galaxy Sample SDSS-I&II	9
3.5	Baryon Oscillation Spectroscopic Survey SDSS-III	9
3.5.1	Intermediate Data Releases DR9-11	10
3.5.2	Final Data Release DR12	11
3.6	Extended Baryon Oscillation Spectroscopic Survey SDSS-IV	12
3.6.1	LRGs	12
3.6.2	ELGs	13
3.6.3	Quasars	14
3.7	WiggleZ Dark Energy Survey	15
4	Results	16
5	Discussion	20
A	Marginalizing over dilation parameters	22

1 Introduction

The quest to understand Dark Energy, the physical mechanism behind observations of the accelerating expansion of the Universe, has led to a plethora of ongoing and future experiments, including the Dark Energy Spectroscopic Instrument (DESI, [1]), the Rubin Observatory and LSST survey [2], and the Euclid [3] and WFIRST [4] satellite missions. Many of these are designed to use the Baryon Acoustic Oscillation (BAO), and Redshift-Space Distortion (RSD) signals within the clustering of galaxies to constrain the geometry of the Universe and growth of structure within it.

Over the past two decades, since the early signs of the baryon acoustic oscillations were seen in the 2-degree Field Galaxy Redshift Survey (2dFGRS, [5]) and the BAO signal was refined using the SDSS-II Luminous Red Galaxy (LRG) sample [6] and the final release of data from the 2dFGRS [7], ground based surveys have been undertaken to make BAO and RSD measurements to ever higher precision. The combination of 2dFGRS and the final SDSS-II LRG data reached a detection threshold of 3.6σ [8], which was rapidly overtaken by early data from the Baryon Oscillation Spectroscopic Survey (BOSS, [9]), which breached the 5σ detection threshold. Since then, the BAO technique has become one of the pillars of

modern cosmology, with particularly important surveys undertaken within the Sloan Digital Sky Survey (SDSS, [10]). At low redshift, we have the Main Galaxy Sample (MGS, [11]) using data from SDSS-I&II ([12]), while at higher redshift we have the SDSS-III ([13]) BOSS, [14] and the SDSS-IV ([15]) extended Baryon Oscillation Spectroscopic Survey (eBOSS, [16]). In addition, complementary measurements were made by the 6-degree Field Galaxy Survey (6dFGS, [17]) at low redshift, and the WiggleZ Dark Energy Survey (WiggleZ, [18]) at high redshift. All have released measurements at various stages of survey progress.

The observed BAO and RSD signals from these surveys have been analyzed by different groups with slightly different techniques in both configuration and Fourier space. These measurements constrain the anisotropic distance scales, D_M and D_H , the isotropic distance scale, D_V , and the logarithmic growth rate of structure, f . The Fisher matrix formalism has allowed cosmologists to predict the constraining power of surveys on these parameters and therefore plan for the future [19–22]. This formalism was first introduced to estimate the error on model parameters in any given dataset [23], by assuming that the inverse of the Fisher matrix can be interpreted as an estimation of the covariance matrix for a Gaussian likelihood. Moreover, the Cramér-Rao inequality states that the diagonal elements of the inverse of the Fisher matrix give a lower bound on the variance of any unbiased estimator of the model parameters, in other words, the best possible errors. Thus, validating the Fisher matrix predictions made for past surveys is important to test whether survey goals were met and particularly to test the optimality of the analysis techniques used to evaluate the cosmological parameters. For instance, in a recent study by Ruggeri et al. [24], the errors in BAO survey measurements, mocks, and Fisher matrix were compared without applying reconstruction to the density field for six galaxy surveys, finding good agreement. We find similar results for the same surveys and datasets analysed in the same way, but extend this analysis to consider further data: BAO with reconstruction and RSD measurements.

The goal of our paper is to compare the constraints recovered from the BAO and RSD measurements of various surveys with the Fisher matrix predictions for the expected error bars. The inputs to the Fisher calculations match as closely as possible that of each analysis. The outline of this paper is as follows. In Section 2, we briefly describe the Fisher matrix formalism and how it is applied in this paper. We continue with descriptions of the surveys considered here in Section 3 and the numbers used throughout this paper. In Section 4, we present our Fisher code results, and then compare them to the observations. In particular, we evaluate these surveys’ performance, comparing the Fisher-predicted errors with the precision recovered from the BAO and RSD measurements. Finally, we discuss the results in Section 5.

2 Methodology

We now briefly describe how we perform the Fisher-based predictions for a given survey. In order to match the experiments, we separately predict errors for BAO and RSD measurements. Before describing the specifics of these calculations, we introduce the general Fisher matrix methodology that is not exclusive to cosmology, but rather can be used for estimating the errors of any given dataset.

Supposing that \vec{x} is a random variable with the probability distribution $f(\vec{x}; \vec{p})$, where \vec{p} is a vector of known parameters, the Fisher information matrix ([19, 25]) corresponding to this set of variables is defined as

$$F_{i,j} \equiv - \left\langle \frac{\partial^2 \ln f}{\partial p_i \partial p_j} \right\rangle. \quad (2.1)$$

Applying this to galaxy surveys, we wish to estimate a set of cosmological parameters $\{p_1, p_2, \dots\}$ using the redshift space galaxy power spectrum, $P(k, \mu)$, and the galaxy number density, n , in the survey's volume, V_{sur} . Following Tegmark (1997) [19], if we let the data vector \vec{x} be the galaxy power spectrum for a Gaussian random field, Eq. 2.1 will yield the following expression for the Fisher matrix:

$$F_{ij} = \frac{V_{\text{sur}}}{4\pi^2} \int_{-1}^1 d\mu \int_{k_{\text{min}}}^{k_{\text{max}}} k^2 dk \mathcal{F}_{ij}(k, \mu), \quad (2.2)$$

where,

$$\begin{aligned} \mathcal{F}_{ij}(k, \mu) &= \frac{1}{2} \left(\frac{V_{\text{eff}}}{V_{\text{sur}}} \right) \frac{\partial \ln P}{\partial p_i} \frac{\partial \ln P}{\partial p_j}, \\ V_{\text{eff}} &= \left[\frac{nP(k, \mu)}{nP(k, \mu) + 1} \right]^2 V_{\text{sur}}, \end{aligned} \quad (2.3)$$

and V_{eff} and μ are the effective volume and the cosine of the angle between \vec{k} and the line of sight. In the linear regime, the power spectrum can be written

$$P = P(k, \mu) = (b + f\mu^2)^2 P_{\text{lin}}(k), \quad (2.4)$$

where b , f , P_{lin} denote the galaxy bias, logarithmic growth rate and linear power spectrum.

We split each survey in N_z slices, and numerically integrate Eq. 2.2 in each redshift slice and eventually add the Fisher matrices to yield the inverse of the total covariance matrix. Moreover, for each survey, we assume the same fiducial cosmology as quoted in their corresponding BAO and RSD measurement paper. For completeness, we list these in Table 1. In Section 2.1 and 2.2 we describe the constraints recovered from BAO and RSD analyses respectively.

2.1 The Fisher matrix for the BAO measurements

To predict the constraints on the parameters recovered from BAO measurements, we adapt the approach described in Seo & Eisenstein [26]. Following their method, we construct the Fisher matrix constraints on angular diameter distance D_M , and the Hubble distance D_H , meaning that the free parameters in Eq. 2.2 are $\{p_1, p_2\} = \{\ln D_M, \ln D_H\}$. These parameters can be related to the BAO dilation parameters as follows

$$\begin{aligned} \alpha_{\perp} &= \frac{D_M(z_{\text{eff}})/r_{\text{drag}}}{D_M^{\text{fid}}(z_{\text{eff}})/r_{\text{drag}}}, \\ \alpha_{\parallel} &= \frac{D_H(z_{\text{eff}})/r_{\text{drag}}}{D_H^{\text{fid}}(z_{\text{eff}})/r_{\text{drag}}}. \end{aligned} \quad (2.5)$$

From these parameters we can further obtain the isotropic volume-averaged distance, $D_V = [zD_H(z)D_M(z)^2]^{1/3}$. The final expression for the Fisher matrix of the anisotropic distances, as described in Seo & Eisenstein, is

$$F_{i,j} = V_{\text{sur}} A_0^2 \int_0^1 d\mu f_i(\mu) f_j(\mu) \int_0^{\infty} dk \frac{k^2 \exp[-2(k\Sigma_s)^{1.4}]}{\left(\frac{P(k)}{P_{0.2}} + \frac{1}{nP_{0.2}R(\mu)}\right)^2} \exp\left[-k^2(1-\mu^2)\Sigma_{\perp}^2 - k^2\mu^2\Sigma_{\parallel}^2\right], \quad (2.6)$$

Table 1: A list of fiducial cosmologies used for each survey in the Fisher analysis.

Survey	Ω_m	Ω_b	h	σ_8	n_s	Ω_ν
6dFGS	0.3	0.0478	0.70	0.82	0.96	0
MGS	0.31	0.048	0.67	0.83	0.96	0
BOSS (DR12)	0.31	0.04814	0.676	0.8	0.97	0
BOSS (DR9-11)	0.274	0.0457	0.70	0.8	0.95	0
eBOSS	0.31	0.04814	0.676	0.8	0.97	0.0014
WiggleZ	0.27	0.04483	0.71	0.8	0.963	0

where $P_{0.2}$ is the galaxy power at $k = 0.2 h \text{ Mpc}^{-1}$, Σ_\perp and Σ_\parallel are the rms radial displacement across and along the line of sight, Σ_s is the inverse of the Silk-damping scale, and A_0 is the normalization of the baryonic term in the Eisenstein & Hu power spectrum [27]. Depending on which element of the Fisher matrix is being calculated, $f_1(\mu) = \mu^2 - 1$ and $f_2(\mu) = \mu^2$. They assumed redshift distortions of the form

$$R(\mu) = (1 + f\mu^2/b)^2 \exp(-k^2\mu^2\Sigma_z^2), \quad (2.7)$$

where f is the logarithmic derivative of the linear growth rate with respect to scale factor, $dD(a)/d\ln(a)$, and b is the galaxy bias. The exponential term corresponds to a Gaussian uncertainty in redshift characterized by Σ_z , which will be discussed more in Section 3.

Since the normalisation and baryon damping terms in the power spectrum $P(k)$ in Eq. 2.6 are functions of Ω_b , Ω_m , and h , it is important to recalculate these for the cosmology assumed if it is different from the default in the version of the code publicly released by Seo & Eisenstein. As we adjust our Fisher calculations to match the cosmology assumed by different authors in their analyses, we have extended the code to allow the relevant parameters to change, using the Eisenstein & Hu (1998) fitting function for the power spectrum. Additionally, since the experimental results that we compare against include reconstruction of the density field to better recover the linear power spectrum (dating back to Peebles [28] and Eisenstein et al. [29]), throughout this paper we need to include it in our Fisher-based analyses as well. Therefore, as an estimation of the reconstruction, we decrease Σ_\parallel and Σ_\perp by 50% following ref. [26] and [29].

2.2 The Fisher matrix for the RSD measurements

In redshift space, the clustering of galaxies is distorted along the line of sight due to peculiar velocities. Measuring these redshift-space distortions (RSD) can provide a estimate of the growth rate of structure. In this Section, we describe how we predict such constraints using the Fisher formalism, following the method described in White et al. [20]. To start with, we consider $\{p_1, p_2\} = \{\ln b\sigma_8, \ln f\sigma_8\}$ as the set of our free parameters. The parameter of interest constraining the structure growth is $f\sigma_8$, where f is the logarithmic growth rate, and σ_8 is the amplitude of fluctuations in an $8 h^{-1} \text{ Mpc}$ radius. For the purpose of this paper the galaxy bias, b , is a nuisance parameter over which we marginalize.

We can rewrite Eq. 2.4 as

$$P = (b\sigma_8(z) + f\sigma_8(z)\mu^2)^2 \frac{P_m(k, z)}{\sigma_8(z)^2}. \quad (2.8)$$

Then after taking the partial derivatives we obtain

$$\begin{aligned}\frac{\partial \ln P}{\partial \ln p_1} &= \frac{2b\sigma_8(z)}{b\sigma_8(z) + f\sigma_8(z)\mu^2}, \\ \frac{\partial \ln P}{\partial \ln p_2} &= \frac{2\mu^2 f\sigma_8(z)}{b\sigma_8(z) + f\sigma_8(z)\mu^2}.\end{aligned}\tag{2.9}$$

By inserting Eq. 2.9 into Eq. 2.3, we can derive the constraints on $f\sigma_8$. In order to provide consistent predictions for all surveys for our baseline RSD-based Fisher predictions we assume that the dilation parameters α_{\parallel} and α_{\perp} are held fixed, rather than marginalizing over them. This limits the dependence on the BAO detection, which in turn controls how well the dilation parameters are constrained. Therefore, our results should not be directly compared to those from measurements where they marginalize over these parameters after performing a joint fit to data.

For many of the surveys, the authors provide errors for both fixed BAO dilation parameters (“as”) and results after marginalizing over them, which we refer to as $f\sigma_8^{\text{fx. as}}$, and $f\sigma_8^{\text{mg. as}}$, respectively. Other analyses provided the covariance matrices for the four parameters, from which we can calculate both. When marginalizing over dilation parameters, we simply take the square root of the $f\sigma_8$ diagonal element in the covariance matrix, $f\sigma_8^{\text{mg. as}} = \sqrt{C_{f\sigma_8, f\sigma_8}}$. To find $f\sigma_8^{\text{fx. as}}$, we calculate the $f\sigma_8$ error from the $f\sigma_8$ diagonal element of the inverse covariance matrix (the survey’s Fisher matrix), $f\sigma_8^{\text{fx. as}} = [C^{-1}]_{f\sigma_8, f\sigma_8}^{-1/2}$. In Section 3, we briefly describe which method is used to set the correct values in Table 2 and Table 3.

2.3 Integration Limits (k_{\min} and k_{\max})

To forecast the Fisher-based analysis parameters, we need to make assumptions about the upper and lower limits of the integral in Eq. 2.2. Each survey is able to extract information up to scales comparable to its size. Formally, the integral constraint affects the power spectrum such that a copy of the window function centred at $k = 0$ is subtracted from the convolved power, leaving zero power at $k = 0$ (e.g. [30]). Thus, information on scales the size of the survey window is not present. To match this behaviour, we choose the lower limit of our integral over scales to be $k_{\min} = 2\pi V_{\text{sur}}^{-1/3}$ ([19, 22]) mimicking the effect of the window with a sharp cut in scales included. The choice of k_{\max} , on the other hand, depends on the scales to which we can extract linear information. The non-linear evolution primarily affects the BAO through well controlled damping terms Σ_{\perp} and Σ_{\parallel} , and thus Seo & Eisenstein [26] suggested that when extracting the BAO parameters, we can set $k_{\max} = 0.5 h \text{Mpc}^{-1}$. Indeed, we find that $\sigma_{\ln D_V}$ is not sensitive to the choice of k_{\max} for $k \gtrsim 0.3 h \text{Mpc}^{-1}$; the BAO provide a large-scale signal localized in configuration space, such that in k -space the signal rapidly diminishes to small scales (See the left panel of Fig. 2). This finding agrees very well with results from N-body simulations [26], which also found that the error is stable for $k_{\max} = 0.3, 0.4$, and $0.5 h \text{Mpc}^{-1}$.

For the RSD measurements, we found that $\sigma_{\ln f\sigma_8}$ is highly dependent on the choice of k_{\max} . On small scales, the density field becomes highly non-Gaussian and hence the inverse of the linear Fisher matrix gives a more optimistic estimation of the error bars than the measurements. The reduction in linear information available is gradual: in models, this results in an increased dependence on non-linear parameters, often allowed to be free given unknown non-linear effects including beyond-linear galaxy bias. The exact scale at which we stop being able to recover linear information is expected to depend on the details of

the galaxy population, and on the accuracy and number of free parameters included in the model used. This problem leads us to test the Fisher error bars' sensitivity to the change of k_{\max} . Our default prediction is to calculate the expected error on $f\sigma_8$ up to a fiducial $k_{\max} = 0.1/D(z = z_i) h \text{ Mpc}^{-1}$ at each redshift slice. This is based on arguments made by Okumura et al. [31], where they showed that after this scale the power spectrum turns strongly non-linear to the extent that a Taylor series cannot adequately describe the redshift-space density field anymore [21].

We also consider inverting the problem and using the data measurements to determine what k_{\max} we should use. To do so, we vary k_{\max} from $0.01/D(z_i)$ up to $0.5/D(z_i)$ and we plot $f\sigma_8$ error against $k_{\max}(z_{\text{eff}})$ in Figure 2. This allows us to translate the constraining power of RSD measurements to an effective k_{\max} at which an equivalent amount of information can be extracted from the linear power spectrum.

3 Data and modelling

In this section, we introduce the surveys on which we perform our Fisher analysis: SDSS-I&II Main Galaxy Sample (MGS), SDSS-III Baryon Oscillation Spectroscopic Survey (BOSS), SDSS-IV extended Baryon Oscillation Spectroscopic Survey (eBOSS), and WiggleZ Dark Energy Survey (WiggleZ). To test our code, we compare to the predictions in Zhao et al. [22] for eBOSS, and find that both codes match in giving very similar results for the same input parameters. In our paper, we are only interested in understanding and matching to the statistical errors and so, where appropriate, we have removed the quoted systematic errors from any combined constraints by subtracting them in quadrature.

Uncertainty in redshift estimation can increase uncertainty in the BAO and RSD features by damping the radial component of the power spectrum (as explained in Section 2). The observations require that $\sigma_v \equiv c\sigma_z/(1+z) \leq 10^{-3}c$ for galaxies at all redshifts. However, the quasar clustering measurements suggest that while this requirement holds true for low redshifts, higher redshifts are prone to higher velocity errors. Therefore, when performing our Fisher analysis on the surveys described in Section 3, we assume that the velocity error for quasars has the following form (Zarrouk et al. [32]):

$$\frac{\sigma_v}{c} = \begin{cases} 10^{-3}, & \text{if } z \leq 1.5 \\ \frac{4}{3} \times 10^{-3}(z - 1.5) + 10^{-3}, & \text{if } z > 1.5 \end{cases}. \quad (3.1)$$

We use $\sigma_v = 10^{-3}c$ for all other tracers, and we include the redshift error in both the RSD and BAO Fisher predictions.

Many of the papers introduced in the following sections use mock catalogues for the following reasons: to estimate systematic errors, to test the model of power spectrum or the correlation function, and to better estimate the covariance matrices from the measurements. Noise in the data may lead to error bars that are larger or smaller than the true constraining power of the survey just by chance. To examine this possibility, we also compare the $f\sigma_8$ constraints on mocks to our Fisher-based errors, where available. In general, the results from the fits to mocks provide error bars similar to those obtained from the data (results are shown in left panel of Figure 3).

3.1 Reconstruction Technique

As already described, the BAO feature can be estimated either by measuring the peak in the correlation function or by the harmonic sequence of oscillations in the power spectrum.

As gravitational forces make structure grow through time, this signature blurs, meaning that the precision at which we can measure the BAO signal decreases. In order to sharpen the broadened BAO signal, various reconstruction methods have been proposed based on the idea of rewinding the motion of galaxies to move them into their original positions. The strong impact of using even simple methods to do this on BAO measurements was first described by Eisenstein et al. ([29, 33]), who proposed a method to shift the galaxies' position by the linear-theory estimated Lagrangian displacement field and showed that this process can increase the precision of the BAO signal. In this section, we discuss some reconstruction methods that have been applied to the data papers that we consider throughout this paper.

A significant difficulty in implementing reconstruction arises because of the RSD, and particularly that the RSD direction changes across a survey. This problem has been solved in recent analyses using two different methods. Padmanabhan et al. [34] implemented a finite-difference routine based solving for the potential on a grid covering the survey's volume. The direction of the RSD signal is allowed to vary for different grid points. Burden et al. [35, 36] instead showed how the simple linear theory based reconstruction method can be undertaken in the Fourier space. To allow for RSD without forcing a global plane-parallel approximation, the code is iterative, removing the estimated RSD signal based on the potential field found in a previous step where no RSD was assumed to be present. The authors also tested their method on CMASS DR11 mocks and found that it converges rapidly, requiring only two iterations.

The way in which reconstruction works is described in more detail in Padmanabhan et al. [37] and one important aspect is that the field be smoothed, with a smoothing scale of between 10 and 15 h^{-1} Mpc [36]. Note that while many techniques also leave a field in which the RSD have approximately been removed, this is not a necessary part of the code and the BAO positions and signal strength do not depend on this. The power spectrum (or correlation function) after reconstruction has a complicated form: ref. [37] suggested that the power spectrum be modeled using three nonlinear damping terms and over three wavelength ranges. Thus, while modelling the full post-reconstruction clustering signal is difficult and may change the shape of the clustering in a hard-to-model way, what is clear is that these reconstruction techniques can decrease Σ_{\parallel} and Σ_{\perp} by 50% for the BAO. Thus if one is only concerned with the BAO signal, allowing for smooth changes in the shape of the power to isolate only this signal removes the pernicious effects of reconstruction. Applying this method to the SDSS DR7 sample showed that it reduces the BAO distance error by a factor of 1.8 [37]. The improvement is not universal, with samples reacting differently to reconstruction [9], but it clearly works to improve the average recovered signal for a set of volumes of the Universe.

The methods described above are relatively simple, relying only on linear physics. More sophisticated techniques offer the promise of increased improvements in the future (e.g. [38–41]). All of the analyses we consider in this paper, except for quasars, used simple methods for reconstruction, and we assume a 50% improvement on Σ_{\parallel} and Σ_{\perp} from this.

3.2 RSD modelling

The amount of information that RSD surveys can extract is limited by modelling the power spectrum or correlation function: the data, at least in 2-point form, does not itself provide information about which scales are linear. Even if the data match a linear model, this does not mean that all of the linear information is present, as cancellation of multiple effects is possible (e.g. Fingers-of-God and non-linear growth in the monopole). Therefore, the fidelity

of the RSD modelling will limit the amount of information extracted. In this section we briefly describe the models used in the data papers that we consider.

Fourier space: The simplest RSD model for the power spectrum was first introduced by Kaiser in 1987 [42]. As it does not include nonlinearities in the halo power spectrum, it is therefore only applicable on large scales. Scoccimarro later constructed a fitting model for RSD in 2004 (Sc.; [43]), as a nonlinear extension to the linear Kaiser model (1987) [42] with two free parameters. Scoccimarro’s extension can include Gaussian and non-Gaussian contributions to the velocity dispersion of large-scale flows. Later in 2010, the matter power spectrum in redshift space was developed by Taruya, Nishimichi, and Saito (TNS; [44]). They added various coefficients to the Scoccimarro’s model to account for nonlinearities between the density field and the velocity field and presented a new power spectrum in redshift space for modeling BAO, including nonlinear gravitational clustering and RSD. The TNS model is amongst the most popular RSD models in Fourier space, of which many of the most recent surveys described in this section make use. Since all of these fitting formulae break down on small scales, they limit their analyses to a maximum k , which is reported as $k_{\max}(\text{O.})$ in Table 2 and 3.

Configuration space: One model that includes nonlinearities in the correlation function in redshift space at quasi-linear scales is the streaming model by Reid & White [45]. They modelled the nonlinear mapping between the real and redshift space with the Gaussian streaming model, in which they included the dependence of halo pairwise velocities on their separation and angle with respect to the line-of-sight. We refer to this RSD model as R+11.

A more realistic way to model RSD in configuration space is to model the intrinsic galaxy clustering and the velocity field with Convolved Lagrangian Perturbation Theory (CLPT; [46]) and then model the convolution of the velocity field along the line-of-sight with the Gaussian Streaming model (GS; [45]). Throughout, we refer to this method as CLPT+GS RSD model. On the other hand, Jennings et al. (J+11; [47]) proposed a cosmology-independent relationship between the velocity field and the density field, from which they found an RSD fitting model based on the nonlinear velocity divergence matter power spectrum. In addition, Sanchez et al. [48] described a simple recipe for modelling the full shape of the clustering wedges that we refer to as S+13. The nonlinear power spectrum in this model is motivated by RPT [49]. A variation of this method, gRPT [50, 51] has also been used by ref. [52].

The maximum wavenumber used in Fourier analyses, as stated before, is given by the so-called k_{\max} . The analogous scale in real space is the smallest scale in the correlation function from which authors can extract information, and is usually referred to as s_{\min} . In our paper, we are interested in comparing the Fisher-based k_{\max} with that of the measurements. For the purposes of Table 2 and Table 3, whenever the analysis is done in configuration space, we approximate k_{\max} with $\sim 1.15\pi/s_{\min}$, based on arguments made by [45]. This allows us to compare the smallest scales used in both real and Fourier space RSD analyses with the effective k_{\max} corresponding to the total amount of linear information available.

3.3 6-degree Field Galaxy Survey

The 6dFGS survey was undertaken from 2001 to 2006 using the Six-Degree Field multi-fibre instrument of the UK Schmidt Telescope (UKST) [53]. This survey covered more than 125,000 galaxies over $\sim 17,000 \text{ deg}^2$ of the southern sky in the redshift range $z < 0.3$ with a median redshift of $z_{\text{med}} = 0.053$.

For the BAO analysis, we use the same catalogue as Carter et al. [54], which contains 75,117 galaxies after applying cuts to the magnitude and the completeness. This catalogue

has an effective redshift of $z_{\text{eff}} = 0.097$ and an effective bias of $b_{\text{eff}} = 1.65$. The early analysis of Beutler et al. [55] was recently supplanted by an analysis that used more modern techniques, including reconstruction from Burden et al. (2014, 2015) with a smoothing scale of $15 h^{-1} \text{Mpc}$ and a covariance matrix based on more sophisticated simulations (i.e. [54]). They found that the 6dFGS likelihood is bimodal, with a 4.6% error on D_V for the best fit model. The authors combined the post-reconstruction 6dFGS with the SDSS MGS sample and reported the lowest fractional error to date on D_V , 3.2%, at low redshift. This favoured the second most likely peak seen when fitting the post-reconstruction BAO signal in the 6dFGS. The 6dFGS sample only adds enough information to provide an improvement of $\sim 16\%$ on the MGS BAO measurements at low redshift. For our analysis we include results from the 6dFGS separately from the MGS as we are interested in the surveys independently.

Beutler et al. in 2012 [56], used a slightly different catalogue containing 81,971 galaxies to make RSD-based measurements. They made use of two RSD models for the 2D correlation function in configuration space, namely, the Simple Streaming model down to $r = 10 h^{-1} \text{Mpc}$ and the Scoccimarro model down to $r = 16 h^{-1} \text{Mpc}$ or $k_{\text{max}} \sim 0.23 h \text{Mpc}^{-1}$ (Sc. in Table 2). We only report the results with the Scoccimarro model as it only fits for the two parameters of interest, $f\sigma_8$ and $b\sigma_8$, and it gives a fractional error on their measurement of $f\sigma_8^{\text{fx.}\alpha\text{s}}$ of 13.0%. Since they do not fit the dilation parameters in their model, we consider their result as if dilation parameters were fixed, i.e, the error on $f\sigma_8^{\text{fx.}\alpha\text{s}}$ is 13.0%, and in Table 2 we do not report the $f\sigma_8^{\text{mg.}\alpha\text{s}}$ for this survey. They also varied their fiducial cosmology without their results changing. This is because the degeneracy between RSD parameters and dilation parameters is very small at low redshift.

3.4 Main Galaxy Sample SDSS-I&II

The Main Galaxy Sample (MGS) is a part of the seventh data release (DR7; [12]) of SDSS I&II ([10]), using observations from the 2.5-meter Sloan telescope located at Apache Point Observatory (APO; Gunn et al. [57]). In this paper, we consider the subsample of 63,163 galaxies covering $6,318 \text{ deg}^2$ of the sky, with a redshift range of $0.07 < z < 0.2$ and an effective bias of 1.5 created by Ross et al. [58]. The MGS sample contains significantly more galaxies than this but, because it was volume limited, a high bias subsample was selected for analysis in order to facilitate the creation of mock catalogues from simulations (which then only required halos to a higher halo mass limit). Ross et al. followed the standard linear reconstruction prescription using the Fourier based method, and found that reconstruction improved the BAO signal by a factor of 2. The post-reconstruction D_V was measured to an accuracy of 3.8%, and there was no evidence of systematic errors. In addition, based on the post-reconstruction BAO measurements and using the CLPT RSD model in range $25 < s < 160 h^{-1} \text{Mpc}$ ($k_{\text{max}} = 0.14 h \text{Mpc}^{-1}$), Howlett et al. [59] measured $f\sigma_8^{\text{fx.}\alpha\text{s}}$ and $f\sigma_8^{\text{mg.}\alpha\text{s}}$ to an accuracy of 31.8% and 40.5% respectively (Table 2, eighth and second case).¹ Moreover, in order to estimate the covariance matrix precisely, 1000 mock catalogues from PICOLA code have been analysed for the MGS sample by Howlett et al. [59]. They found that the best fit value from the average of these mocks gives $f\sigma_8^{\text{fx.}\alpha\text{s}} = 0.5_{-0.12}^{+0.13}$. (Table 1, 8th case).

3.5 Baryon Oscillation Spectroscopic Survey SDSS-III

The Baryon Oscillation Spectroscopic Survey (BOSS) [14] is a part of the SDSS-III [13] that was undertaken by the 2.5-meter Sloan Telescope from 2008 to 2014. Covering an area of

¹Since the error bars in this analysis are asymmetric, we average the upper and lower error bars.

10,000 deg², BOSS contains more than 1.5 million galaxies with redshifts up to $z = 0.7$. Two target selection algorithms were used to create the BOSS galaxy sample: LOWZ (at lower redshift) is a selection of luminous red galaxies to $z \approx 0.4$, and CMASS (for constant stellar Mass) covers LRGs up to a higher redshift range $z \lesssim 0.7$ [60]. We review the catalogue selection and the BAO and RSD measurements in three early data releases of BOSS, DR9, DR10, and DR11 in Section 3.5.1, and the final data release DR12, in Section 3.5.2.

3.5.1 Intermediate Data Releases DR9-11

The BOSS DR9 CMASS sample contains 264,283 galaxies in a region of 3,275deg² of the sky. Galaxies used in this catalogue cover a redshift range of $0.43 < z < 0.7$ with an effective redshift of $z_{\text{eff}} = 0.57$. BAO measurements were presented by Anderson et al. [9] and showed that $\sigma \ln D_V = 1.6\%$. Anderson et al. used the finite difference reconstruction method with a smoothing scale of $15 h^{-1} \text{Mpc}$, and found that applying reconstruction to this particular data does not improve the precision of the BAO feature. They suggested that this is because the pre-reconstruction errors of this sample were already at the lower end of the expected range (from mocks)—hence there was little for reconstruction to improve. RSD measurements for this survey were presented in Reid et al. [61] providing fractional error bars on the growth rate $f\sigma_8^{\text{mg. as}} = 14.6\%$ and $f\sigma_8^{\text{fx. as}} = 8.1\%$. For both of these analyses, the systematic errors were negligible compared to the statistical errors. Their findings show that $b\sigma_8(z_{\text{eff}}) = 1.2$, where $\sigma_8(z_{\text{eff}}) = 0.61$, which gives an effective bias of 2.0. They fit the monopole and quadrupole moments of the correlation function down to scales of $s_{\text{min}} = 25 h^{-1} \text{Mpc}$ (or $k_{\text{max}} \sim 0.14 h \text{Mpc}^{-1}$) with Reid & White’s RSD model [45].

BOSS Data Release 10 (DR10) contains 218,905 galaxies in LOWZ ($0.15 < z < 0.43$) and 501,844 galaxies in CMASS ($0.43 < z < 0.7$). Using these catalogues, D_V was constrained to 2.8% and 1.4% for LOWZ and CMASS, respectively, by Anderson et al. [62]. They also measured the anisotropy distances for CMASS in this catalogue and found a consensus ($P(k) + \xi(s)$) error of 1.9% and 5.0% on D_M and D_H , respectively. Anderson et al. [62] also analyzed the 11th data release of BOSS, which consists of 313,780 galaxies in LOWZ and 690,826 galaxies in CMASS. This gave a statistical consensus ($P(k) + \xi(s)$) error of 2.0% and 0.9% on D_V for LOWZ and CMASS, respectively (after subtracting 0.3% systematic error in quadrature). They also found errors of 1.4% and 3.5% for the anisotropic distances, D_M and D_H , respectively. For both DR10 and DR11 data, the reconstruction method by Padmanabhan et al. was applied to NGC and SGC separately.

Sanchez et al. [63] constrained the logarithmic growth of structure using the 10th and 11th BOSS data releases, using the S+13 model described earlier, within the range of $40 h^{-1} \text{Mpc} < s < 160 h^{-1} \text{Mpc}$ or a k_{max} of $0.09 h \text{Mpc}^{-1}$. They found fractional errors of 23.3%, 12.8%, 20.8%, and 10.8% on $f\sigma_8^{\text{mg. as}}$, for LOWZ DR10, CMASS DR10, LOWZ DR11, and CMASS DR11, respectively.

Since Sanchez et al. did not publish either the $f\sigma_8^{\text{fx. as}}$, nor the covariance matrix including growth rate and dilation constraints for BOSS DR10 and DR11 samples, we are limited in how well we can replicate these results. Therefore, we use the CMASS DR11 RSD measurements from Samushia et al. [64] instead. These used the RSD streaming model described in Reid & White (R+11, [45]) with $s_{\text{min}} = 25 h^{-1} \text{Mpc}$ or $k_{\text{max}} \sim 0.14 h \text{Mpc}^{-1}$, finding errors of 9.9% and 6.0% on $f\sigma_8^{\text{mg. as}}$ and $f\sigma_8^{\text{fx. as}}$ respectively, which we include in Table 3. Systematic errors have been ignored in this analysis since they have been checked with mocks and they had less than a 1% effect. When fitted to growth of structure separate from the dilation

parameters, they found $b\sigma_8 = 1.26$, which gives an effective bias of $b(z_{\text{eff}}) = 2.05$ given that $\sigma_8(z = 0.57) = 0.615$.

3.5.2 Final Data Release DR12

To determine the Fisher-based predictions for the final data release of BOSS, DR12, we follow the data selection method of two studies. First, Alam et al. [65] who split this sample by redshift range (Near and Mid in Table 2) and second, Gil-Marín et al. [66], who studied the LOWZ and CMASS catalogues separately (LZ and CM in Table 3). In the following, we discuss the recovered errors for BAO and RSD measurements for both selection methods.

Alam et al. combined LOWZ with CMASS, and after applying redshift cuts to the combined sample, they created three partially overlapping redshift samples that cover 9329 deg² area of the sky. In this paper, we refer to the first redshift bin, at $0.2 < z < 0.5$, which mainly consists of the LOWZ galaxy sample, as the near redshift bin, and the second redshift bin at $0.4 < z < 0.6$, mainly consisting of the CMASS sample, as the mid redshift bin, with effective redshifts $z_{\text{eff},1} = 0.38$ and $z_{\text{eff},2} = 0.51$ respectively. In our work, we do not consider the higher redshift bin at $0.5 < z < 0.75$ of the BOSS survey, as it is combined with the eBOSS LRG samples (refer to Section 3.6.1). According to Table 3 in Beutler et al., BOSS has an effective bias of 2.03, and 2.13 in the LOWZ and CMASS samples. Note that the Luminous Red Galaxy (LRG) samples in this paper are assumed to have a galaxy bias of $b_{\text{LRG}}(z) = 1.7/D(z)$, where $D(z)$ is the linear growth factor. This assumption is consistent with the fiducial bias assumed in Zhao et al. [67] and Prakash et al. [68], as well as the effective biases measured for the LOWZ and CMASS samples.

The post-reconstruction BAO-only analysis by Alam et al. yields a 1.5%, 2.7%, and 1.0% statistical uncertainty in D_M , D_H , D_V for the BOSS Near sample. For the BOSS Mid sample, these uncertainties are lower: 1.4%, 2.3% and 0.9% for D_M , D_H , and D_V respectively. They used the reconstruction method described in Padmanabhan et al. For the constraint on the growth rate, Alam et al. incorporated results from 4 different papers, using different methods: real-space multipoles (Satpathy et al. [69]; CLPT+GS, $s_{\text{min}} = 25 h^{-1}$ Mpc), real-space wedges (Sanchez et al. [50]; similar to TNS, $s_{\text{min}} = 20 h^{-1}$ Mpc), Fourier-space multipoles (Beutler et al. [30]; TNS, $k_{\text{max}} = 0.15 h$ Mpc⁻¹), and Fourier-space wedges (Grieb et al. [52]; gRPT+RSD, $k_{\text{max}} = 0.2 h$ Mpc⁻¹). The BAO+FS consensus measurements from all of these works yield a 7.8% statistical error on $f\sigma_8^{\text{mg.}\alpha\text{s}}$ for the near redshift bin, and 7.6% for the mid redshift bin. We utilized the covariance matrix to obtain the constraint on $f\sigma_8^{\text{fx.}\alpha\text{s}}$, which is 7.0% for the near redshift slice and 6.4% for the mid redshift slice.

In addition, BOSS DR12 measured BAO ([70]) and RSD ([66]) using LOWZ and CMASS samples, consisting of 361,762, and 777,202 galaxies within the redshift ranges $0.15 < z < 0.43$, and $0.43 < z < 0.70$, and with effective redshifts of 0.32, and 0.57. They found that $b\sigma_8$ for these two samples are 1.29 and 1.24, resulting in an effective bias of 1.9 and 2.1, respectively. Throughout their study, they have made use of the finite-difference reconstruction method by Padmanabhan et al.

The BAO-only consensus analysis in real space and Fourier space have shown errors of 2.2%, 5.9%, and 1.7% on D_M , D_H , and D_V in the LOWZ sample, and 1.3%, 2.9%, and 0.9% on D_M , D_H , and D_V in the CMASS sample (Table 4 in [70]). Moreover, after modelling the RSD with the TNS model with a k_{max} of $0.24 h$ Mpc⁻¹, Gil-Marín et al. [66] measured $f\sigma_8^{\text{mg.}\alpha\text{s}}$ with an error of 15.7% and 8.6%, and when assuming no AP effect, they measured

$f\sigma_8^{\text{fx. as}}$ with an error of 9.1% and 5.0% in LOWZ and CMASS samples respectively (Table 3 in [66]).

3.6 Extended Baryon Oscillation Spectroscopic Survey SDSS-IV

The extended Baryon Oscillation Spectroscopic Survey (eBOSS; Dawson et al.) [16] is a part of SDSS-IV (Blanton et al. [15]), and used the Sloan Telescope at Apache Point Observatory (APO; Gunn et al. [57]) to conduct a redshift survey at higher redshifts than BOSS from 2014 to 2019. From this survey’s 16th data release, we use the DR16 Luminous Red Galaxy (LRG [71]; Section 3.6.1), Emission Line Galaxy (ELG [72]; Section 3.6.2), and Quasar samples ([73]; Section 3.6.3), which are reported in Table 2. We have also used the LRG and Quasar samples from an earlier data release, DR14 (Pâris et al. [74]), which are reported in Table 3. Since for eBOSS the systematic errors are estimated using mock catalogues, in this section we only quote the statistical error bars.

3.6.1 LRGs

There are 174,816 LRGs in eBOSS DR16 sample that cover 9,493 deg² of the night sky, with an effective redshift of $z_{\text{eff}} = 0.698$. For LRGs in the redshift range $0.6 < z < 1.0$, we combine the eBOSS LRG sample with 202,642 CMASS BOSS DR12 galaxies, to be consistent with the Bautista et al. [75] constraints. We want the Fisher forecast to have the same effective bias as the full MCMC fit to the TNS model, which is $b_1 = 2.2$. Therefore, we assume that the linear bias has the form of $1.5/D(z)$.

The estimated covariance matrix reported by Bautista et al. [75], for the BAO-only analysis, after applying the reconstruction technique of Burden et al. [35, 36], showed that the fractional statistical errors on D_M , D_H , and D_V , are 1.6%, 2.5%, and 1.6% respectively.

For obtaining the growth rate, they used CLPT+GS RSD to model correlation function in real space and combined their results with the Fourier-space analysis of Gil-Marín et al. [76], which used the TNS model. In this paper we use their consensus results. They tested for different fitting ranges of scales, and found that the optimal minimum scales that should be covered in the CLPT+GS and TNS model are $25 h^{-1} \text{Mpc}$ ($k_{\text{max}} \sim 0.14 h \text{Mpc}^{-1}$) and $20 h^{-1} \text{Mpc}$ ($k_{\text{max}} \sim 0.18 h \text{Mpc}^{-1}$), respectively.

The consensus BAO + Full Shape RSD fit indicated that the error on $f\sigma_8^{\text{mg. as}}$ and $f\sigma_8^{\text{fx. as}}$ are 9.4% and 9.1% (from eq. 56 in ref. [75]). In Table 10 of Bautista et al. they evaluated the systematic errors using mocks, and showed that the systematic error of $f\sigma_8$ for CLPT and TNS is 0.024 and 0.023 respectively. If we subtract ~ 0.0235 from the total error obtained from Eq. 56, in quadrature, then we obtain an error of 7.9% and 7.6% on $f\sigma_8^{\text{mg. as}}$ and $f\sigma_8^{\text{fx. as}}$. Furthermore, for this catalogue, they constructed 1000 EZmock realisations for the LRG eBOSS+CMASS survey geometry and obtained 9.9% error on $f\sigma_8^{\text{fx. as}}$ in the mocks, which is shown in Figure 3.

An earlier data release of the eBOSS LRG sample, DR14, when combined with CMASS, is comprised of 126,557 galaxies in redshift range $0.6 < z < 1.0$, with an effective redshift $z_{\text{eff}} = 0.720$. Bautista et al. [77] followed the reconstruction technique presented by Burden et al. [35, 36], and the post-reconstruction BAO measurement analysed by them showed a 2.5% fractional error on D_V . The anisotropic fits on this data shows very different upper and lower error bars: $D_M = 2689_{-79}^{+158}$, and $D_H = 2593_{-589}^{+177}$. Hence we do not report these errors in Table 3. But the isotropic fit shows that $D_V = 2377_{-59}^{+61}$ which translates into 2.5% fractional error. The RSD measurement for this sample has been modeled with CLPT+GS model by Icaza-Lizaola et al. [78] on scales $28 < s < 124 h \text{Mpc}^{-1}$ ($k_{\text{max}} = 0.13 h \text{Mpc}^{-1}$)

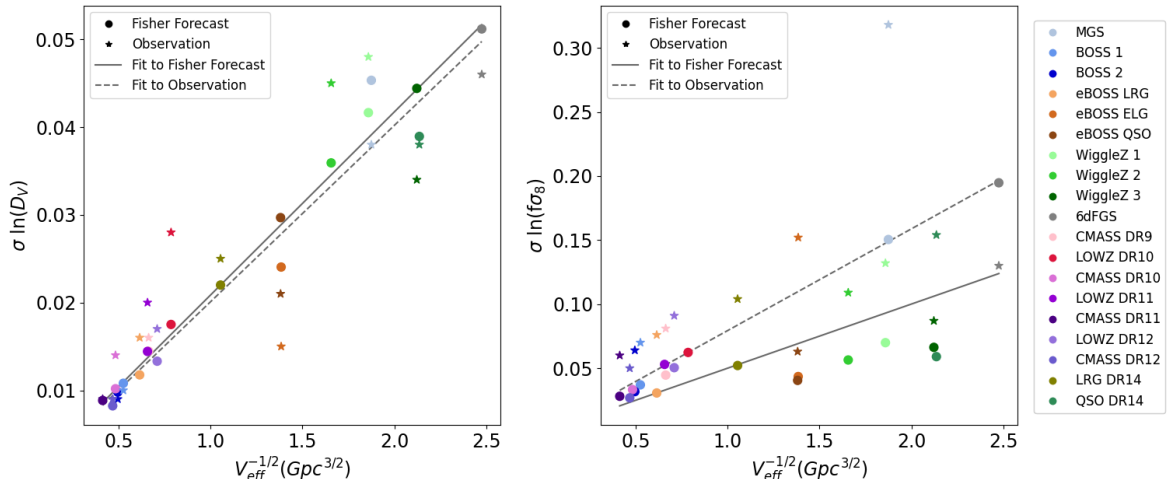


Figure 1: D_V fractional error as measured from the BAO position plotted against the effective volume $V_{\text{eff}}^{-1/2}$ for different surveys (left panel). A clear trend is seen, with the slopes of the linear fit to the Fisher and observational errors being 0.022 and 0.020, respectively. The measured RSD constraints show a weaker correlation with $V_{\text{eff}}^{-1/2}$.

and they found a fractional error of 29.2% on $f\sigma_8^{\text{mg.}\alpha\text{s}}$. Using the covariance matrix of their analysis, we found a fractional error of 10.4% for $f\sigma_8^{\text{fx.}\alpha\text{s}}$. Their fit showed that $b\sigma_8 = 1.11$ (Table B1 in ref. [78]), which means assuming $D(z_{\text{eff}} = 0.72) = 0.691$, the effective bias would be $b_{\text{eff}} = 2.0$. We therefore use the functional form of $1.4/D(z)$ for bias evolution in our Fisher analysis.

3.6.2 ELGs

The 16th data release of SDSS-IV contains 173,736 Emission Line Galaxies (ELGs) covering an effective area of 727 deg² at effective redshift $z_{\text{eff}} = 0.845$ in the redshift range $0.6 < z < 1.1$ (de Mattia et al. [79] & Tamone et al. [80]). Tamone et al. fitted for galaxy bias and found that $b = 1.52$. Therefore, for this sample, we assume a galaxy bias function of $b_{\text{ELG}}(z) = 0.99/D(z)$, as $D(z_{\text{eff}} = 0.85) = 0.651$.

De Mattia et al. applied the iterative FFT reconstruction method introduced by Burden et al. and assumed a Gaussian smoothing scale of 15 h^{-1} Mpc. The isotropic BAO measurements in Fourier space for this sample gave statistical upper error of 2.5% and lower error of 2.8% for D_V , which is a factor of 1.2 smaller than the total errors. We averaged the upper and lower error bars for reporting in Table 2 (refer to Table 9 of ref. [79] for statistical-only errors).

They also performed the Fourier space BAO+RSD measurements using the TNS model in the fitting range $0.03 < k < 0.2 h \text{Mpc}^{-1}$ for the monopole. However, at the end they combined their results with the configuration space result from Tamone et al. [80], which used the CLPT+GS RSD model with $s_{\text{min}} = 32 h^{-1}$ Mpc or equivalently, $k_{\text{max}} \sim 0.11 h \text{Mpc}^{-1}$. Statistical only errors on $f\sigma_8^{\text{mg.}\alpha\text{s}}$, D_H , and D_M as calculated by de Mattia et al., are 23.4%, 9.0%, and 3.9%, whereas Tamone et al. obtained 23.9%, 9.1%, and 4.6%, respectively. Combining these two measurements we find statistical fractional errors of 23.6%, 9.0% and 4.3% on $f\sigma_8^{\text{mg.}\alpha\text{s}}$, D_H , and D_M . Since the ELG likelihood in the BOSS DR16 sample cannot be adequately approximated with a Gaussian, instead of using the covariance matrix to fix

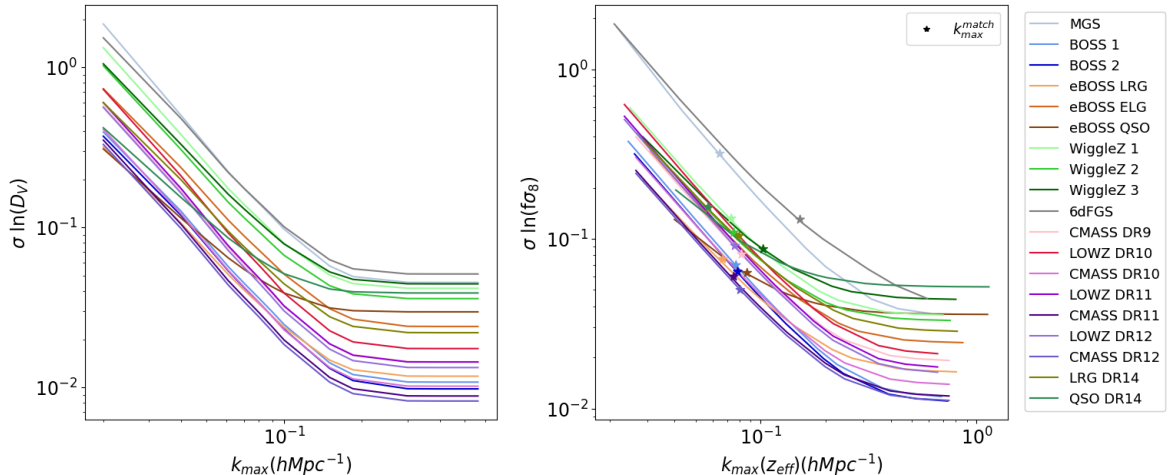


Figure 2: The Fisher-based predicted fractional error on D_V (left) and $f\sigma_8$ (right) plotted against $k_{\max}(z = z_{\text{eff}})$ for different surveys. Note that in contrast to the $f\sigma_8$ error, the D_V error converges to a constant at $k \gtrsim 0.3 h\text{Mpc}^{-1}$. The stars on the right panel indicate the k_{\max} at which the Fisher prediction and the experiment are equal.

the dilation parameters, we use the supplied probability grid in D_M and D_H , measuring the error on $f\sigma_8$ when D_M and D_H are constrained within a small range around their best-fit values. By doing so, we find a 15.2% error on $f\sigma_8^{\text{fx.}\alpha\text{s}}$. De Mattia et al. tested their analysis using different mock catalogues and found that the baseline Global Integral Constraint model (baseline, GIC) gives an 11.5% error on $f\sigma_8^{\text{fx.}\alpha\text{s}}$, which is shown in Figure 2.

3.6.3 Quasars

Quasar samples are of significant interest when it comes to constraining parameters at high redshift. In this study, we include the eBOSS DR16 sample containing 343,708 Quasars covering 4,699 deg^2 in the redshift range $0.8 < z < 2.2$, with an effective redshift of $z_{\text{eff}} = 1.48$ (Neveux et al. [81]). According to Croom et al. [82], the quasar bias can be approximated as $b(z)_{\text{QSO}} = 0.53 + 0.29(1+z)^2$, which gives an effective bias of 2.31. Taking the average of best fits on $b_{1,\text{NGC}}\sigma_8$ and $b_{1,\text{SGC}}\sigma_8$ from their Table 10, and dividing by $\sigma_8(z_{\text{eff}} = 1.48) = 0.41$, implies that the best fit effective bias is 2.33, which is very similar to the Croom formula. Note that BAO reconstruction is not applied to quasars, as their density is too low to provide us with an adequate estimate of the matter density field.

BAO-only measurements by Neveux et al. [81] in Fourier space, combined with those from configuration space by Hou et al. [83], gives the consensus errors of 2.6%, 4.1%, and 1.6% for D_M , D_H , and D_V (Table 6 in [81]). By subtracting the systematic errors in quadrature, according to their Table 5, we find that these numbers change only slightly, and become 2.5%, 4.0%, and 1.5% for D_M , D_H , and D_V .

Neveux et al. [81] used the TNS model for RSD measurements within the range $0.02 < k < 0.3 h\text{Mpc}^{-1}$, and obtained a 9.9% error on $f\sigma_8^{\text{mg.}\alpha\text{s}}$. Whereas Hou et al. [83] introduced a new method similar to TNS in order to model the correlation function within the scale range of $20 < s_{\text{min}} < 160 h^{-1}\text{Mpc}$ ($k_{\max} \sim 0.18$), and found a 10.9% error on $f\sigma_8^{\text{mg.}\alpha\text{s}}$. When combining the two to find a consensus result, this reduced to 9.7%. Considering that both of these papers estimated that the systematic error is about 30% of the statistical error, that

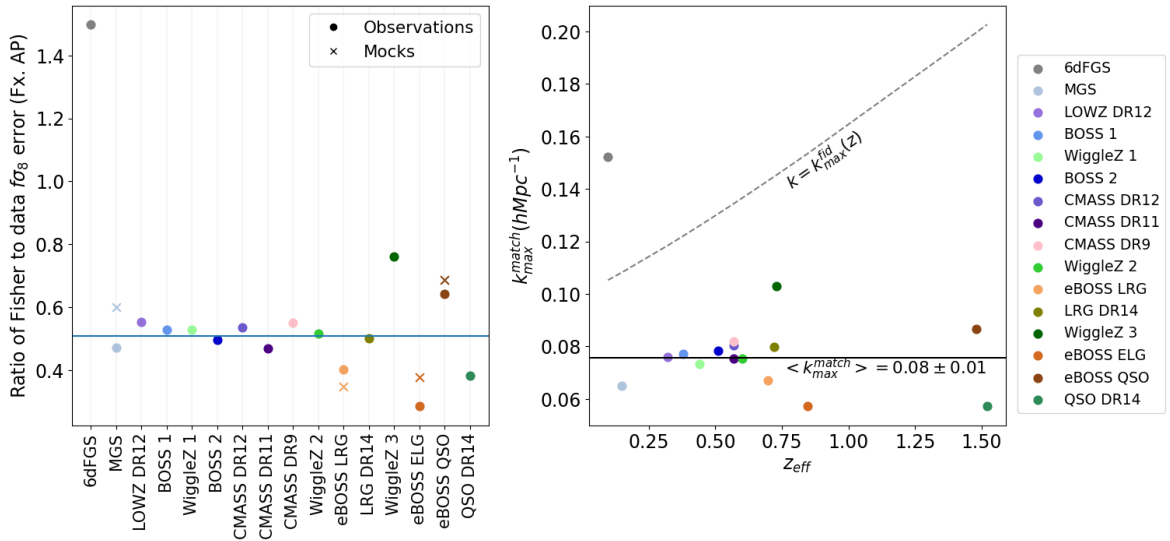


Figure 3: *Left:* The difference between Fisher-based prediction $f\sigma_8$ error and observational $f\sigma_8^{\text{fx.}\alpha\text{s}}$ error is plotted for each survey. The x markers indicate mock errors instead of the errors obtained from observations. *Right:* We have adjusted the k_{max} in order to make Fisher predictions match with the experiments. The dashed line represents the fiducial value of $k_{\text{max}} = 0.1/D(z) h \text{ Mpc}^{-1}$. Note that the fiducial cosmology used to draw this line is the same as the BOSS cosmology. (WiggleZ Near, Mid, and Far redshift slices are shortened as 1, 2, and 3)

gives a final only-statistical error of 9.3% on $f\sigma_8^{\text{mg.}\alpha\text{s}}$. After fixing the dilation parameters using the covariance matrix for the full shape analysis, and subtracting the 30% systematic error in quadrature, we found that $f\sigma_8^{\text{fx.}\alpha\text{s}}$ should have an error of 6.3%. Neveux et al. made use of 1000 EZmocks to estimate the covariance matrix and the observational systematic errors that we reported above. From these mocks catalogues, they recovered $f\sigma_8 = 0.467$, with an average fractional error of 0.059, which is shown with a brown cross in Figure 3.

In addition, we also run our Fisher-code for the eBOSS DR14 Quasar sample, consisting of 148,659 galaxies with redshifts $0.8 < z < 2.2$ and an effective redshift of $z_{\text{eff}} = 1.52$, and a footprint of $2,113 \text{ deg}^2$. The BAO measurement for this sample showed a 3.8% fractional error on D_V , considering that the systematic errors are negligible for this sample (Ata et al. [84]). The RSD measurement fitting the CLPT+GS model for scales larger than $s_{\text{min}} = 20 h^{-1} \text{ Mpc}$ ($k_{\text{max}} \sim 0.18 h \text{ Mpc}^{-1}$) showed a 16.4% fractional statistical error on $f\sigma_8^{\text{mg.}\alpha\text{s}}$. After taking systematic effects into account, the combined error rose to 18.5%. From the covariance matrix provided, this translates to a 15.4% error on $f\sigma_8^{\text{fx.}\alpha\text{s}}$ (Table 9 of Zarrouk et al. [32], stat. error). Zarrouk et al. also fitted for the galaxy bias and found that $b\sigma_8 = 1.038$, or $b(z_{\text{eff}} = 1.52) = 2.6$. In our Fisher code, we re-scaled the Croom formula by a factor of 1.1 to match this bias.

3.7 WiggleZ Dark Energy Survey

The WiggleZ Dark Energy Survey was undertaken using the 3.9-meter Anglo-Australian Telescope (AAT; Drinkwater et al. [85]). This survey observed approximately 240,000 ELGs over the redshift range $0.2 < z < 1.0$ from 2006 to 2011. We consider the final data release that covers 816 deg^2 in the sky in six regions, and contains 158,741 ELGs. Following the analyses

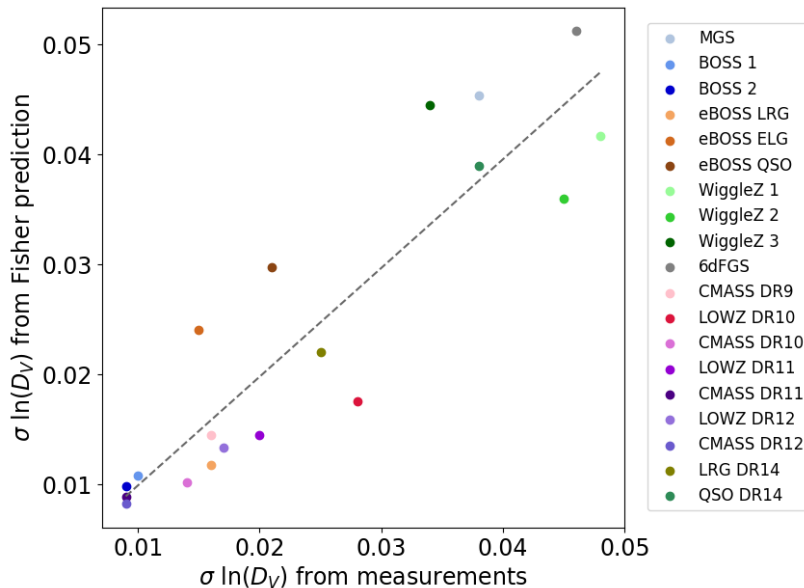


Figure 4: The Fisher-based predicted fractional error on D_V plotted against the fractional error recovered from BAO-only analysis. The slope of the fitted line is 1.1, which implies that the Fisher prediction and the BAO measurements are in good agreement.

of Blake et al. [86] and Kazin et al. [87], we first combine these six regions together and divide the galaxies into three partially overlapping redshift bins $0.2 < z_{\text{near}} < 0.6$, $0.4 < z_{\text{mid}} < 0.8$, and $0.6 < z_{\text{far}} < 1.0$, and then analyze each catalogue separately. Throughout our Fisher analysis, we assume that the galaxy bias is $b_{\text{ELG}} = 0.8/D(z)$, to match the effective biases as assumed when performing reconstruction as in Kazin et al., in each redshift bin ($b_{\text{eff}} = 1.0$, 1.1, and 1.2 in Near, Mid, and Far, respectively)

Kazin et al. [87], found that after applying the reconstruction method by Padmanabhan et al., D_V has an uncertainty of 4.8%, 4.5% and 3.4% at effective redshifts $z_{\text{eff}}^{\text{Near}} = 0.44$, $z_{\text{eff}}^{\text{Mid}} = 0.60$, and $z_{\text{eff}}^{\text{Far}} = 0.730$, respectively. Additionally, Blake et al. [86], fitted with the RSD model introduced by Jennings et al. [47] (J+11), and for $k < 0.2 h \text{ Mpc}^{-1}$ found a fractional error on $f\sigma_8^{\text{mg.}\alpha\text{s}}$ of 19.4%, 16.1%, and 16.4% for the near, middle, and far redshift slices, respectively. When fixing the dilation parameters, the fractional error bars reduce to $f\sigma_8^{\text{fx.}\alpha\text{s}} = 13.2\%$, 10.9%, and 8.7%.

4 Results

We have performed a Fisher matrix analysis to predict BAO and RSD errors for the surveys introduced in Section 3, matching the parameters assumed for the Fisher calculations as closely as we can to the parameters of the surveys. The final results of our calculations on the fractional error of the cosmological parameters, D_M , D_H , D_V , and $f\sigma_8$, for each survey’s final data release and for BOSS and eBOSS intermediate data releases, are presented in Table 2 and Table 3, respectively (abbreviated as F.). For comparison, we also present the errors of D_M , D_H , D_V from the BAO measurements published in the most recent analyses of the data, with errors calculated using sets of mock catalogues (abbreviated as O. for observed). In addition, we present the fractional errors of $f\sigma_8$ from the most recent RSD analysis of the

data, when dilation parameters are marginalized over (abbreviated as Mg. αs), and when they were held fixed (abbreviated as Fx. αs). The RSD predictions depend strongly on the value of k_{\max} adopted, which is the upper limit of the integration in Eq. 2.2. In the penultimate rows in Table 2 and 3, we present $k_{\max}^{\text{fid}} = 0.1/D(z_{\text{eff}})$, matching the assumptions previously made for many surveys (e.g. [22]), and k_{\max}^{match} , that we will describe in detail later in this section.

In these tables, the effective redshift, z_{eff} , is the weighted mean redshift, using weights $w_{\text{FKP}} = (1 + \bar{n}P_0)^{-1}$ from Feldman et al. [88]. The effective area, A_{eff} , is the survey’s area as reported from its corresponding clustering catalogue documentation. The effective volume is calculated from the equation below,

$$V_{\text{eff}} = V_{\text{survey}} \sum_{i=1}^{N_z} \left(\frac{n(z_i)P_0}{1 + n(z_i)P_0} \right)^2, \quad (4.1)$$

where P_0 is the amplitude of the power spectrum at $k \sim 0.15 h \text{ Mpc}^{-1}$. Its value for 6dFGS, MGS, BOSS DR12 and eBOSS LRGs is 10,000, for eBOSS ELGs is 4,000, for eBOSS Quasars is 6,000, for BOSS DR9-12 is 20,000 and for WiggleZ is 5,000, all in units of $h^{-3} \text{ Mpc}^3$.

For the combined 6dFGS and MGS samples, we obtain a 3.1% accuracy on D_V , very similar to the 3.2% error reported by Carter et al. [54] for the combined samples. In Table 2, only the constraints recovered from the 6dFGS sample are reported, since we are interested in the surveys separately. Note that 6dFGS and MGS do not geometrically overlap more than 3%, allowing their Fisher matrices to be added directly to obtain the final constraint at low redshift. Additionally, Alam et al. used the combined CMASS+LOWZ BOSS catalogue over the redshift range $0.2 < z < 0.75$, split into three partially overlapping catalogues in redshift covering $0.2 < z < 0.5$, $0.4 < z < 0.6$, and $0.5 < z < 0.75$ and measured the BAO and RSD parameters in each of these bins separately. In this paper we did not analyze the high redshift bin separately since we combined the high redshift BOSS LRGs with the eBOSS LRGs to match the catalogue used by Bautista et al. These two samples geometrically overlap in the eBOSS footprint, and that is why we needed to calculate the overlapping area and the non-overlapping area separately and add the Fisher matrices to obtain the errors reported in Table 2.

In the following, we briefly describe the key results that our analysis implies.

- From the left panel in Figure 1, we are able to confirm that there is a linear relationship between the fractional error on D_V and $V_{\text{eff}}^{-1/2}$, as expected from Eq. 2.6, both for observations and predictions. The Fisher-based D_V errors were calculated under the assumption of $k \gtrsim 0.5 h \text{ Mpc}^{-1}$. From the left panel in Figure 2, we found that $\sigma_{\ln D_V}$ is not sensitive to the choice of k_{\max} for $k \gtrsim 0.3 h \text{ Mpc}^{-1}$ (Section 2.3 for more detail on the k_{\max} choice). Furthermore, we obtained similar slopes for the Fisher analysis and observations, showing that the Fisher method works well, and that observational methods are able to extract information reaching close to the maximum possible. In addition, Figure 4 supports this claim by revealing a linear relationship, with a slope very close to unity, between the measured D_V error and the Fisher-predicted D_V error.
- Table 2 and 3 show that our Fisher prediction of fractional error on the volume averaged distance from the BAO measurements, σ_{D_V}/D_V , deviates less than 35% from analyses

Table 2: The Fisher forecast (shortened as F.) errors for D_M , D_H , D_V , and $f\sigma_8$ compared to the errors from the BAO and RSD measurements (shortened as O.). The RSD rows show $f\sigma_8$ errors from observations with and without marginalisation over the dilation parameters (Mg. for marginalized and Fx. for fixed). For 6dFGS, the sample used for RSD has slightly different b_{eff} and z_{eff} from the sample used for BAO; in the Fisher forecast we use b_{eff} and z_{eff} from ref. [54] for both, for consistency. The BOSS analysis have used 4 different RSD models that were briefly described in the text. The eBOSS LRG⁺ sample reported in this table is the combined eBOSS LRG sample covering 4,242 deg² with the BOSS DR12 sample at high redshift ($0.6 < z < 1.0$), covering 9,494 deg². We also display the k_{max} of the observations (converted from configuration to Fourier space if applicable); the fiducial Fisher k_{max} ; the k_{max} at which the Fisher RSD constraints match the observations; the RSD model used; whether the fit was performed in configuration (*s*) or Fourier (*k*) space; and the references for the RSD and BAO papers.

	6dFGS	MGS	BOSS		eBOSS			WiggleZ		
			Near	Mid	LRG ⁺	ELG	QSO	Near	Mid	Far
z_{eff}	0.097	0.15	0.38	0.51	0.698	0.845	1.48	0.44	0.600	0.73
$A_{\text{eff}}(\text{deg}^2)$	17000	6813	9329	9329	4242	727	9494	816	816	816
$V_{\text{eff}}(\text{Gpc}^3)$	0.134	0.282	3.401	4.082	2.652	0.522	0.525	0.288	0.364	0.223
b_{eff}	1.65	1.5	2.03	2.13	2.2	1.52	2.33	1.0	1.1	1.2
Fractional errors from the BAO analysis (in percent)										
D_M (O.)			1.5	1.4	1.6	4.3	2.5			
D_M (F.)	8.0	6.4	1.5	1.3	1.7	3.6	3.4	6.9	6.0	7.5
D_H (O.)			2.7	2.3	2.5	9.0	4.0			
D_H (F.)	16.1	13.8	3.1	2.8	3.2	6.3	5.0	11.3	9.5	11.4
D_V (O.)			1.0	0.9	1.6	2.7	1.5	4.8	4.5	3.4
D_V (F.)	5.8	4.9	1.1	1.0	1.2	2.5	3.0	4.6	3.9	4.9
BAO ref.	[54]	[58]	[65]	[65]	[75]	[79]	[81]	[87]	[87]	[87]
Fractional errors from the RSD analysis (in percent)										
$f\sigma_8$ (O.Mg.)		40.5	7.8	7.6	7.9	23.6	9.3	19.4	16.1	16.4
$f\sigma_8$ (O.Fx.)	13.0	31.8	7.0	6.4	7.6	15.2	6.3	13.2	10.9	8.7
$f\sigma_8$ (F.Fx.)	19.5	15.0	3.7	3.2	3.1	4.4	4.0	7.0	5.6	6.6
k_{max} for the RSD modeling										
k_{max} (O.)	0.23	0.14	0.17	0.17	0.16	0.16	0.24	0.2	0.2	0.2
k_{max} (Fid. F.)	0.11	0.11	0.12	0.13	0.14	0.15	0.20	0.12	0.13	0.14
k_{max} (Match)	0.16	0.06	0.08	0.08	0.07	0.06	0.08	0.07	0.07	0.11
RSD Model	Sc.	CLPT	4 Models		TNS&CLPT+GS			J+11		
RSD space	<i>s</i>	<i>s</i>	<i>k/s</i>	<i>k/s</i>	<i>s</i>	<i>k/s</i>	<i>k/s</i>	<i>k</i>	<i>k</i>	<i>k</i>
RSD ref.	[56]	[59]	[65]	[65]	[75]	[79]	[81]	[86]	[86]	[86]

that use similar techniques, including reconstruction and covariance matrices calculated using mock catalogues. We consider this to be an exceptionally positive result for the field of BAO analyses, showing that current methods are extracting all of the available signal (i.e. reconstruction is working as well as expected in Seo & Eisenstein, with a 50%

drop in Σ_s). Better reconstruction methods (e.g. [38–40]) would be able to improve the BAO constraints by reducing the non-linear damping.

- The picture is worse for RSD-based measurements: If we assume that $k_{\max} = k_{\max}^{\text{fid}}$, the $f\sigma_8$ fractional error is not very well estimated by the Fisher matrix analysis, and it shows a lower correlation with the effective volume than D_V (Figure 1; right panel). In our baseline Fisher calculation, we assume that the dilation parameters are fixed. Therefore, we choose the $f\sigma_8$ errors taken from observations to be those for which the dilation parameters D_M and D_H were fixed. We have been able to adjust most of the measurements we have considered to match the baseline assumed for the Fisher predictions. Whether or not we marginalise has a big effect on the results, and so it is important to match Fisher with observations.
- The $f\sigma_8$ error is highly dependent on the choice of maximum k to which we integrate to make Fisher predictions and hence from which we can recover information. Decreasing k_{\max} weakens the predicted constraints on $f\sigma_8$ (Figure 2; right panel). For most of the catalogues used in this work, we calculated the k_{\max}^{match} that, when used in the Fisher analysis, gives an $f\sigma_8$ error that matches with that of the experiments. The average of k_{\max}^{match} over these catalogues is about $0.08 \pm 0.01 h \text{ Mpc}^{-1}$, with remarkably little scatter around this value. This should be interpreted as the amount of linear information that can be recovered from these data.

If the theoretical arguments that led to expecting k_{\max}^{fid} to increase at higher redshifts hold true, then the data analyses are missing significant information, particularly at high redshift. Alternatively, the theoretical arguments are wrong, possibly because the high bias of the samples analysed at high redshift shifts the non-linear scale to lower k . Either way, this is clearly an area where improved modeling is required (e.g. [89–95]).

- The right and left panels of Figure 3 show a consistent story. The left panel shows that the ratio of Fisher-predicted to observed $f\sigma_8$ error generally decreases to higher redshift (note that the samples are arranged from low to high redshift). The right hand panel shows that to match the observed information, we need k_{\max}^{match} to stay fixed, while k_{\max}^{fid} increases with redshift. The quasars are least consistent with this trend, with a relatively better agreement between Fisher and observations, but a strong change in k_{\max} . Figure 2 explains why this is: it shows that, for the low galaxy density of the quasar sample, there is increasingly little information on small scales due to the high shot noise. A large value of k_{\max}^{fid} brings in less expected information (the green and brown curves are flatter, showing that for eBOSS DR14 and DR16 QSO information saturates quickly). This makes it even more interesting that, for all samples, the information recovered on $f\sigma_8$ is that predicted by the Fisher analysis to a consistent k_{\max}^{match} , despite large differences in shot noise, bias, and redshift.
- Our baseline results are presented assuming that the dilation parameters are fixed. We have also considered the alternative of marginalizing over unknown dilation parameters, using the sample itself, predominantly through the BAO signal to constrain these. We compare this alternative procedure for both the data and the Fisher matrix. In general, we find a better agreement between the Fisher and data for this procedure: comparing with the case of fixed dilation parameters shows that fixing the α s does not constrain $f\sigma_8$ as much in the data as in the Fisher. We suggest that the reason for this is that

when modeling the data we have other parameters fitted (e.g. shot noise, nonlinear bias parameters), and so our $f\sigma_8$ errors assuming fixed dilation do not reach their theoretical minima. That is, for the Fisher calculation, we reach a precision when we fix the dilation parameters that goes beyond that achievable in the data for other reasons.

Marginalising over the dilation parameters leads to more scatter in the ratio of the Fisher-based error on $f\sigma_8^{\text{mg.}\alpha\text{s}}$ to the data error. We also find a small shift in the value of $k_{\text{max}}^{\text{match}}$ required to match Fisher and data: marginalising over the dilation parameters, we find $k_{\text{max}}^{\text{match}} = 0.09 \pm 0.02 h \text{ Mpc}^{-1}$. The increased scatter leads to an error on $k_{\text{max}}^{\text{match}}$ of $0.02 h \text{ Mpc}^{-1}$ which is twice as large for fixed dilation parameters. This can be seen by eye comparing Figure 5 to Figure 3. This is likely because in the data, imperfect measurement of the BAO peak adds an extra source of scatter in the marginalized $f\sigma_8$ errors. Hence our fiducial comparison uses $f\sigma_8$ errors with fixed dilation parameters, which are thus less noisy. In summary, our conclusion remains unchanged when considering $f\sigma_8^{\text{mg.}\alpha\text{s}}$; we still do not see the error decrease to high redshift, as one would naively expect. The exact prescription we use for marginalising over the dilation parameters is presented in Appendix A.

- By considering the average measurement recovered from mock catalogues, we are able to remove the statistical error from the measurements: i.e. the actual observation is only one realization of what could have happened in that particular region of the universe, and therefore its constraints can depend on how lucky the experiment was. For the MGS, eBOSS LRG, eBOSS ELG, and eBOSS Quasar experiments, the teams created 1000 mock catalogues and released the results of fitting the models to them, finding an $f\sigma_8$ error of 25.0%, 8.8%, 11.5%, and 5.9%, respectively. We plotted the ratio of Fisher forecast to the $f\sigma_8$ error recovered from both observations and mocks, if available, in the left panel of Figure 3. We see that the trends seen between Fisher predictions and measurements are well matched between data and mocks. This suggests that the trends are due to the methodology (particularly the model used to fit to the data) rather than statistical fluctuations.

5 Discussion

We have performed a Fisher analysis for 19 different survey catalogues to obtain the constraints on the co-moving angular diameter distance, D_M , the Hubble distance, D_H , and the growth rate of structure $f\sigma_8$, from BAO and RSD analyses. Furthermore, the statistical errors derived were compared for each catalogue to that recovered in recent analyses modelling the correlation function (or the power spectrum). We only selected studies that adopted similar methodologies, using covariance matrices for the 2-point measurements created using mock catalogues, and for BAO measurements using a basic reconstruction method (except for the quasar samples where reconstruction does not improve the BAO signal).

Our Fisher-based BAO and RSD predictions are well matched to those from Zhao et al. [22] for the eBOSS survey if we correct for the difference between predicted and actual survey parameters (area, galaxy redshift distribution, galaxy bias). The differences between predicted and actual survey details make less than a 60% change on the measured errors. By comparing the final measurements with Fisher predictions using the actual eBOSS details, we

Table 3: Same as Table 2, but including intermediate data releases of BOSS and eBOSS. LOWZ and CMASS are shortened as LZ and CM.

	BOSS DR9	BOSS DR10 LZ CM	BOSS DR11 LZ CM	BOSS DR12 LZ CM	eBOSS DR14 LRG+ QSO	eBOSS DR16 LRG+ QSO
z_{eff}	0.57	0.32 0.57	0.32 0.57	0.32 0.57	0.72 1.52	0.698 1.48
$A_{\text{eff}}(\text{deg}^2)$	3275	5156 6161	7341 8377	8337 9376	1845 2113	9494 4699
$V_{\text{eff}}(\text{Gpc}^3)$	2.474	1.770 4.669	2.527 6.381	2.185 5.034	0.910 0.218	2.652 0.525
b_{eff}	2.0	1.8 2.11	1.85 2.05	1.9 2.1	2.0 2.63	2.2 2.33
Fractional errors from the BAO analysis (in percent)						
$D_M(\text{O.})$	2.0	1.9	1.4	2.2 1.3	1.6 2.5	
$D_M(\text{F.})$	2.2	2.7 1.6	2.2 1.4	2.0 1.3	3.2 5.2	1.7 3.4
$D_H(\text{O.})$	3.8	5.0	3.5	5.9 2.9	2.5 4.0	
$D_H(\text{F.})$	4.4	5.4 3.1	4.5 2.7	4.2 2.5	5.9 7.8	3.2 5.0
$D_V(\text{O.})$	1.6	2.8 1.4	2.0 0.9	1.7 0.9	2.5 3.8	1.6 1.5
$D_V(\text{F.})$	1.6	2.0 1.1	1.6 1.0	1.5 0.9	2.2 3.9	1.2 3.0
BAO ref.	[9]	[62] [62]	[62] [62]	[70] [70]	[77] [84]	[75] [81]
Fractional errors from the RSD analysis (in percent)						
$f\sigma_8(\text{O.Mg.})$	14.6	23.3 12.8	20.8 9.9	15.7 8.6	29.2 16.4	7.9 9.3
$f\sigma_8(\text{O.Fx.})$	8.1		6.0	9.1 5.0	10.4 15.4	7.6 6.3
$f\sigma_8(\text{F.Fx.})$	4.5	6.2 3.3	5.3 2.8	5.0 2.7	5.2 5.9	3.1 4.0
k_{max} for the RSD modeling						
$k_{\text{max}}(\text{O.})$	0.14	0.09 0.09	0.09 0.14	0.17 0.17	0.13 0.18	0.16 0.24
$k_{\text{max}}(\text{Fid. F.})$	0.13	0.12 0.13	0.12 0.13	0.12 0.13	0.15 0.20	0.14 0.20
$k_{\text{max}}(\text{Match})$	0.08		0.07	0.08 0.08	0.08 0.07	0.07 0.08
RSD Model	R+11		R+11	TNS	CLPT+GS	TNS&CLPT
RSD space	s	s s	s s	k k	s s	s k/s
RSD ref.	[61]	[63] [63]	[63] [64]	[66] [66]	[78] [32]	[75] [81]

find that the Fisher predictions and observational results are within 30% of each other for all samples for errors on D_V . In contrast, for RSD we find that in general, the errors predicted from our Fisher analysis are about 50% of those of the observations.

Using Fisher-based predictions for the BAO constraints on the BOSS Near sample ($0.2 < z < 0.5$), Dawson et al. [14] predicted a 1% error on D_M and a 1.8% error on D_H , and from their results it can be inferred that the error on D_V is about 1.0%, which is in a good agreement with our Fisher-prediction for BOSS DR12 Near sample. After the BOSS DR9 was released, Font-Ribera et al. [21] performed a Fisher matrix analysis and found 7.0% fractional error on $f\sigma_8$ and 1.15% fractional error on D_V for DR9 CMASS.

More accurate RSD techniques allow for extracting RSD information to smaller scales. For instance, Reid et al. [96] were able to extend the RSD analysis to scales of $0.8 h^{-1} \text{Mpc}$ in configuration space, using an HOD to model the small-scale RSD, and found 2.4% accuracy on $f\sigma_8$ in the BOSS CMASS DR10 sample. This is a factor of 1.4 smaller than our Fisher matrix prediction using $k_{\text{max}}^{\text{fid}} = 0.132$. For the Fisher-based analysis to be as small as this error, we would need to include linear information to $k_{\text{max}}^{\text{match}} = 0.19 h \text{Mpc}^{-1}$. Additionally,

using small scale RSD modelling, Lange et al. [97] extracted the RSD information down to scales of about $0.4 h^{-1} \text{Mpc}$ for two volume-limited catalogues created from the BOSS LOWZ sample in the North Galactic Cap. They found a precision of 5.1% and 5.8% on $f\sigma_8$ at effective redshifts of 0.25 and 0.4, respectively. Our Fisher code, when run on their catalogue with the fiducial $k_{\text{max}} = 0.114$ and $0.123 h \text{Mpc}^{-1}$, yields an error of 11.8% and 9.8% on $f\sigma_8$. This implies that $k_{\text{max}}^{\text{match}}$ should be $0.23 h \text{Mpc}^{-1}$ and $0.14 h \text{Mpc}^{-1}$, respectively. This shows that improved small-scale modelling can extract information to smaller scales than the apparently-universal $k_{\text{max}} = 0.08 h \text{Mpc}^{-1}$ we found for the large-scale analyses. However, ensuring that the RSD modelling remains unbiased on very small scales remains a challenge.

Our analyses suggest that Fisher matrix calculations are very good at predicting BAO constraints, and that measurements and the way in which they are analysed are delivering the expected level of precision. This is clearly great news for future projects. The same could be true for RSD if k_{max} is chosen correctly—our work suggests that current methods extract RSD information to a fixed k_{max} for all samples and redshifts. For both measurements, there is room for improvement—particularly with reconstruction for BAO, and fully extracting the linear signal from which to measure RSD.

It is possible to interpret the consistent k_{max} as indicating that the models fitted do not allow for an increase in the linear information at higher redshift, rather than the information being missing. Indeed, recent analyses using emulators to extract information from smaller scales have been able to provide strong improvements on the precision obtained from RSD [95, 97–99]. The improvement from small-scale analyses shows that the information is available, and improved modelling may be able to extract it.

Acknowledgments

We would like to thank Mariana Vargas Magana and Richard Neveux for providing the covariance matrices for eBOSS Quasars, and Chris Blake and Hector Gil-Marín for thoughtful comments and useful discussions. Special acknowledgment to Yuting Wang who provided code and results for eBOSS Quasar DR14 for comparison to our results. This research made use of the PYTHON packages NUMPY (Walt, Colbert & Varoquaux 2011; [100]), SCIPY (Jones et al.; [101]), MATPLOTLIB (Hunter 2007; [102]), COLOSSUS (Benedikt Diemer; 2018 [103]), and ASTROPY (Astropy Collaboration 2013; [104]). This research was enabled in part by support provided by Compute Ontario (www.computeontario.ca) and Compute Canada (www.computecanada.ca). Research at Perimeter Institute is supported in part by the Government of Canada through the Department of Innovation, Science and Economic Development Canada and by the Province of Ontario through the Ministry of Colleges and Universities.

A Marginalizing over dilation parameters

Our baseline, throughout this paper, when analyzing the $f\sigma_8$ constraint with RSD, is to fix the dilation parameters. In this section, we show that our conclusions remain unchanged if we instead marginalize over the dilation parameters. Considering the free parameters in the Fisher matrix in Eq. 2.1 to be $\{\alpha_{\perp}, \alpha_{\parallel}, \ln f\sigma_8, \ln b\sigma_8\}$, we can build a 4 by 4 Fisher matrix using the following derivatives ([105]):

$$\begin{aligned}
\frac{\partial \ln P}{\partial \alpha_{\perp}} &= -2 + 4f\sigma_8(z)\mu^2(1 - \mu^2)/(b\sigma_8(z) + f\sigma_8(z)\mu^2) - (1 - \mu^2)\frac{\partial \ln P}{\partial \ln(k)}, \\
\frac{\partial \ln P}{\partial \alpha_{\parallel}} &= -1 - 4f\sigma_8(z)\mu^2(1 - \mu^2)/(b\sigma_8(z) + f\sigma_8(z)\mu^2) - \mu^2\frac{\partial \ln P}{\partial \ln(k)}, \\
\frac{\partial \ln P}{\partial \ln f\sigma_8} &= \frac{2\mu^2 f\sigma_8(z)}{b\sigma_8(z) + f\sigma_8(z)\mu^2}, \\
\frac{\partial \ln P}{\partial \ln b\sigma_8} &= \frac{2b\sigma_8(z)}{b\sigma_8(z) + f\sigma_8(z)\mu^2}.
\end{aligned} \tag{A.1}$$

Although we are fitting to the α s, and relying on the BAO signal to constrain these, we follow the standard approach and assume that reconstruction cannot be used, because we also wish to model the form of the clustering signal - something that is hard to do post-reconstruction. Thus, our errors on α will be larger than those in Table 2 and 3, where a standard reconstruction technique was applied to both Fisher prediction and the data. Assuming $k_{\max}^{\text{fid}} = 0.1/D(z) h \text{ Mpc}^{-1}$, we predict errors for these free parameters. The fractional error for $f\sigma_8^{\text{mg}\cdot\text{as}}$ is reported in Table 4 and Table 5. Figure 5 is analogous to Figure 3, except that it is calculated for $f\sigma_8^{\text{mg}\cdot\text{as}}$. As can be seen from this plot, the scatter around the Fisher to data ratio is larger compared to Figure 3, and therefore, so is the scatter around k_{\max}^{match} .

We show contour plots for the data and Fisher matrices (with $k_{\max} = 0.09 h \text{ Mpc}^{-1}$) for few representative samples, spanning a range in redshift and omitting some samples for clarity. We show BOSS DR12 Near (left panel Figure 6), eBOSS+CMASS LRG DR16 (right panel Figure 6), eBOSS Quasar DR16 (left panel Figure 7), WiggleZ Mid (right panel Figure 7), and, eBOSS Quasar DR14 (Figure 8), and eBOSS ELG (Figure 9). The centres of these contours are set to the fiducial value for each parameter. If $b\sigma_8$ was not provided in the data covariance matrix, we omitted the $b\sigma_8$ contour for that survey.

Table 4: The fractional error of $f\sigma_8^{\text{mg}\cdot\text{as}}$ in percent and the k_{\max} at which observed (O.) and Fisher (F.) errors match. In contrast to Table 2, the Fisher prediction errors are calculated after marginalizing over the dilation parameters (Mg.).

	6dFGS	MGS	BOSS		eBOSS			WiggleZ		
			Near	Mid	LRG ⁺	ELG	QSO	Near	Mid	Far
$f\sigma_8(\text{O.Mg.})$	-	40.5	7.8	7.6	7.9	23.6	9.3	19.4	16.1	16.4
$f\sigma_8(\text{F.Mg.})$	-	30.1	7.8	6.7	6.5	7.9	7.3	11.5	9.5	11.4
$k_{\max}(\text{Match})$	-	0.084	0.122	0.117	0.113	0.060	0.104	0.083	0.086	0.094

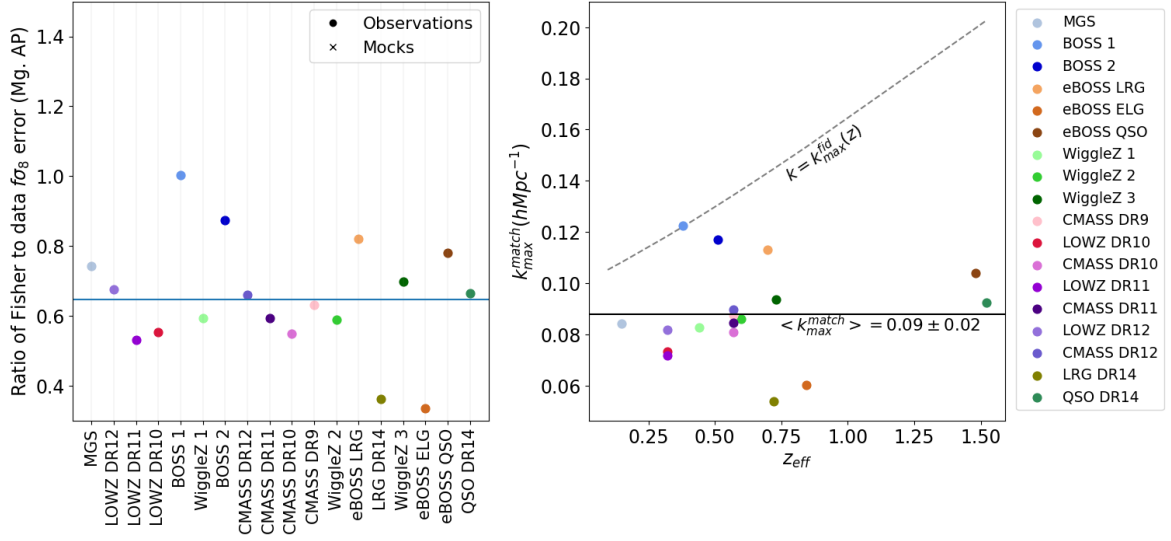


Figure 5: *Left:* The difference between Fisher-based predicted $f\sigma_8$ error and observational $f\sigma_8^{\text{mg. os}}$ error is plotted for each survey. *Right:* We have adjusted the k_{max} in order to make Fisher predictions match with the experiments. The dashed line represents the fiducial value of $k_{\text{max}} = 0.1/D(z) h \text{Mpc}^{-1}$. (Near, Mid, and Far redshift slices are shortened as 1, 2 and 3, respectively.)

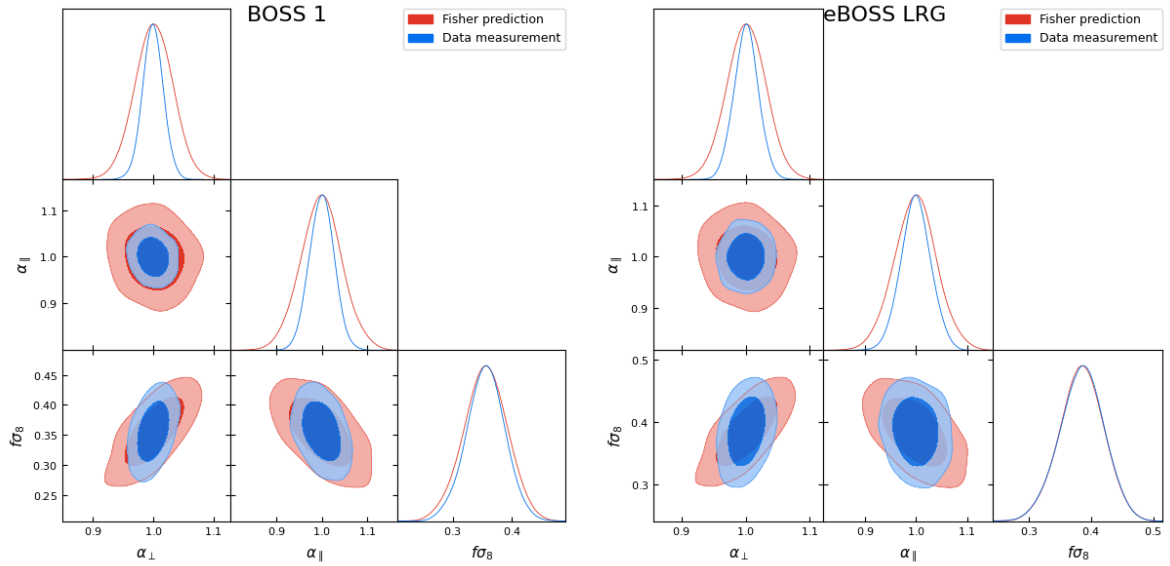


Figure 6: Constraints on α_{\perp} , α_{\parallel} , and $f\sigma_8$. Red contours show 68 and 95 percent confidence regions for the Fisher analysis with $k_{\text{max}} = 0.09 h \text{Mpc}^{-1}$ (this work). *Left:* The full-shape consensus analysis of the BOSS Near DR12 sample is shown in blue (Alam et al. [65]). *Right:* The full-shape RSD analysis for eBOSS LRG DR16 in configuration space analysis is shown in blue (Bautistia et al. [75]).

Table 5: Same as Table 4 but including intermediate data releases.

	BOSS	BOSS DR10		BOSS DR11		BOSS DR12		eBOSS DR14		eBOSS DR16	
	DR9	LZ	CM	LZ	CM	LZ	CM	LRG ⁺	QSO	LRG ⁺	QSO
$f\sigma_8(\text{O.Mg.})$	14.6	23.3	12.8	20.8	9.9	15.7	8.6	29.2	16.4	7.9	9.3
$f\sigma_8(\text{F.Mg.})$	9.2	12.9	7.0	11.1	5.9	10.6	5.7	10.5	10.9	6.5	7.3
$k_{\text{max}}(\text{Match})$	0.087	0.073	0.081	0.072	0.085	0.082	0.090	0.054	0.093	0.113	0.104

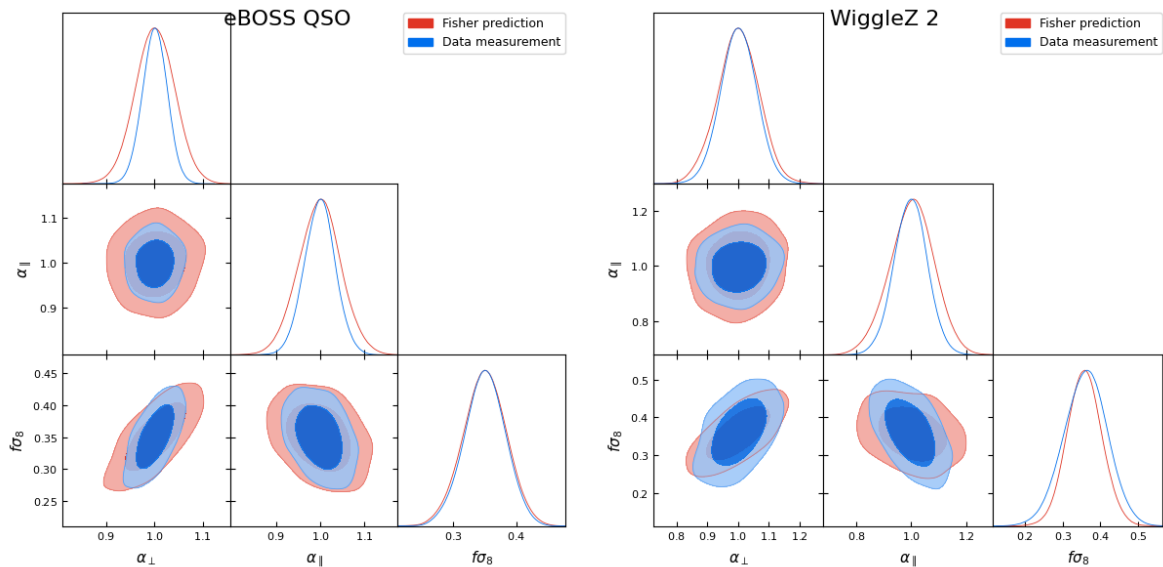


Figure 7: Constraints on α_{\perp} , α_{\parallel} , and $f\sigma_8$. Red contours show 68 and 95 percent confidence regions for the Fisher analysis with $k_{\text{max}} = 0.09 h \text{Mpc}^{-1}$ (this work). *Left:* The full-shape RSD analysis of the eBOSS Quasar DR16 sample is shown in blue (Neveux et al. [81]). *Right:* The joint fit to expansion and growth for WiggleZ Mid redshift slice is shown in blue. The covariance matrix was originally in $\{A, F, f\sigma_8\}$ but then we converted to α_{\parallel} , α_{\perp} and $f\sigma_8$ (Blake et al. [86]).

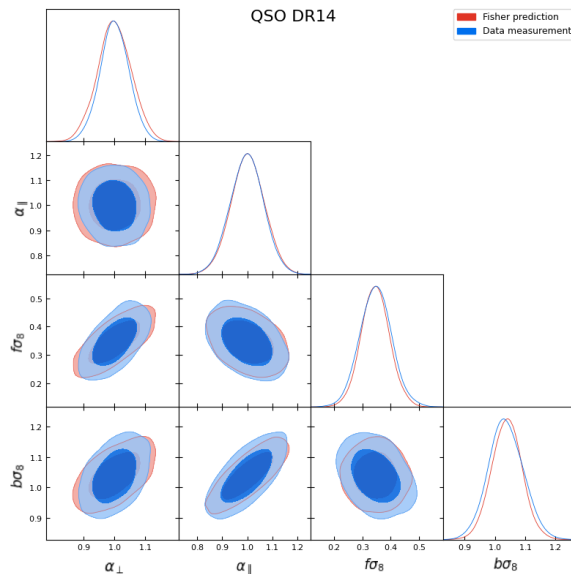


Figure 8: Constraints on α_{\perp} , α_{\parallel} , $f\sigma_8$, and $b\sigma_8$. Red contours show 68 and 95 percent confidence regions for the Fisher analysis with $k_{\max} = 0.09 h \text{ Mpc}^{-1}$ (this work), and the blue contours show confidence regions for eBOSS Quasar DR14 sample analysis from 5-parameter RSD modeling by Zarrouk et al. [32].

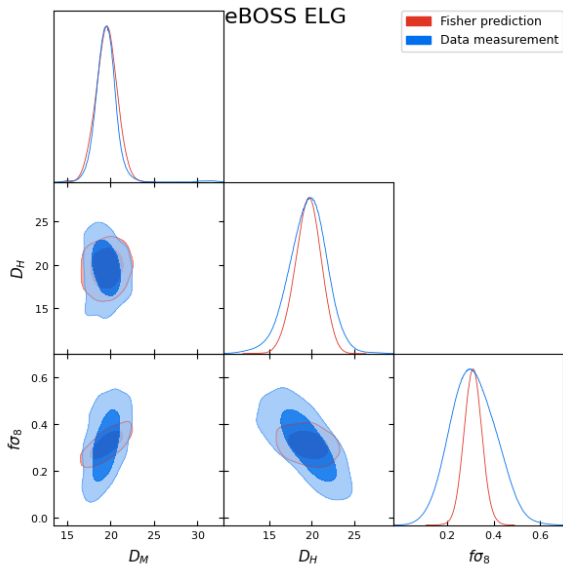


Figure 9: Constraints on D_M , D_H , $f\sigma_8$. Red contours show 68 and 95 percent confidence regions for the Fisher analysis with $k_{\max} = 0.09 h \text{ Mpc}^{-1}$ (this work), and the blue contours show confidence regions for eBOSS ELG sample [79]. Unlike other surveys, data and Fisher do not match very well in eBOSS ELG contour, as for this survey, we found that $k_{\max}^{\text{match}} = 0.06 h \text{ Mpc}^{-1}$, which is far from the average value: $k_{\max} = 0.09 h \text{ Mpc}^{-1}$. For data, the grid of the relative probability has been used instead of the covariance matrix, as the ELG likelihood is not well-approximated as a Gaussian distribution.

References

1. DESI Collaboration, Aghamousa, A., Aguilar, J., *et al.* The DESI Experiment Part I: Science, Targeting, and Survey Design. en. *arXiv:1611.00036 [astro-ph]*. arXiv: 1611.00036. <http://arxiv.org/abs/1611.00036> (2021) (Dec. 2016).
2. LSST Dark Energy Science Collaboration. Large Synoptic Survey Telescope: Dark Energy Science Collaboration. en. *arXiv:1211.0310 [astro-ph, physics:hep-ex]*. arXiv: 1211.0310. <http://arxiv.org/abs/1211.0310> (2021) (Nov. 2012).
3. Euclid Collaboration, Blanchard, A., Camera, S., *et al.* Euclid preparation: VII. Forecast validation for Euclid cosmological probes. en. *A&A* **642**. arXiv: 1910.09273, A191. ISSN: 0004-6361, 1432-0746. <http://arxiv.org/abs/1910.09273> (2020) (Oct. 2020).
4. Spergel, D., Gehrels, N., Baltay, C., *et al.* Wide-Field Infrared Survey Telescope-Astrophysics Focused Telescope Assets WFIRST-AFTA 2015 Report. *arXiv e-prints*, arXiv:1503.03757. arXiv: [1503.03757 \[astro-ph.IM\]](http://arxiv.org/abs/1503.03757) (Mar. 2015).
5. Percival, W. J., Baugh, C. M., Bland-Hawthorn, J., *et al.* The 2dF Galaxy Redshift Survey: The power spectrum and the matter content of the universe. en. *arXiv:astro-ph/0105252*. arXiv: astro-ph/0105252. <http://arxiv.org/abs/astro-ph/0105252> (2021) (May 2001).
6. Eisenstein, D. J., Zehavi, I., Hogg, D. W., *et al.* Detection of the Baryon Acoustic Peak in the Large-Scale Correlation Function of SDSS Luminous Red Galaxies. en. *ApJ* **633**. arXiv: astro-ph/0501171, 560–574. ISSN: 0004-637X, 1538-4357. <http://arxiv.org/abs/astro-ph/0501171> (2021) (Nov. 2005).
7. Cole, S., Percival, W. J., Peacock, J. A., *et al.* The 2dF Galaxy Redshift Survey: Power-spectrum analysis of the final dataset and cosmological implications. en. *Monthly Notices of the Royal Astronomical Society* **362**. arXiv: astro-ph/0501174, 505–534. ISSN: 00358711, 13652966. <http://arxiv.org/abs/astro-ph/0501174> (2021) (Sept. 2005).
8. Percival, W. J., Reid, B. A., Eisenstein, D. J., *et al.* Baryon Acoustic Oscillations in the Sloan Digital Sky Survey Data Release 7 Galaxy Sample. en. *Monthly Notices of the Royal Astronomical Society* **401**. arXiv: 0907.1660, 2148–2168. ISSN: 00358711, 13652966. <http://arxiv.org/abs/0907.1660> (2021) (Feb. 2010).
9. Anderson, L., Aubourg, E., Bailey, S., *et al.* The clustering of galaxies in the SDSS-III Baryon Oscillation Spectroscopic Survey: Baryon Acoustic Oscillations in the Data Release 9 Spectroscopic Galaxy Sample. en. *Monthly Notices of the Royal Astronomical Society* **427**. arXiv: 1203.6594, 3435–3467. ISSN: 0035-8711, 1365-2966. <http://arxiv.org/abs/1203.6594> (2021) (Dec. 2012).
10. York, D. G. The Sloan Digital Sky Survey: Technical Summary. en. *The Astronomical Journal* **120**. arXiv: astro-ph/0006396, 1579–1587. ISSN: 00046256. <http://arxiv.org/abs/astro-ph/0006396> (2021) (Sept. 2000).
11. Strauss, M. A., Weinberg, D. H., Lupton, R. H. & Narayanan, V. K. Spectroscopic Target Selection in the Sloan Digital Sky Survey: The Main Galaxy Sample. en. *The Astronomical Journal* **124**. arXiv: astro-ph/0206225, 1810–1824. ISSN: 00046256, 15383881. <http://arxiv.org/abs/astro-ph/0206225> (2021) (Sept. 2002).

12. Abazajian, K. The Seventh Data Release of the Sloan Digital Sky Survey. en. *ApJS* **182**. arXiv: 0812.0649, 543–558. ISSN: 0067-0049, 1538-4365. <http://arxiv.org/abs/0812.0649> (2021) (June 2009).
13. Eisenstein, D. J., Weinberg, D. H., Agol, E., *et al.* SDSS-III: Massive spectroscopic surveys of the distant Universe, the Milky Way, and extra-solar planetary systems. en. *The Astronomical Journal* **142**, 72. ISSN: 0004-6256, 1538-3881. <https://iopscience.iop.org/article/10.1088/0004-6256/142/3/72> (2021) (Sept. 2011).
14. Dawson, K. S., Schlegel, D. J., Ahn, C. P., *et al.* The Baryon Oscillation Spectroscopic Survey of SDSS-III. en. *The Astronomical Journal* **145**. arXiv: 1208.0022, 10. ISSN: 0004-6256, 1538-3881. <http://arxiv.org/abs/1208.0022> (2021) (Jan. 2013).
15. Blanton, M. R. Sloan Digital Sky Survey IV: Mapping the Milky Way, Nearby Galaxies, and the Distant Universe. en. *The Astronomical Journal*, 35 (2017).
16. Dawson, K. S., Kneib, J.-P., Percival, W. J., *et al.* THE SDSS-IV EXTENDED BARYON OSCILLATION SPECTROSCOPIC SURVEY: OVERVIEW AND EARLY DATA. en. *The Astronomical Journal* **151**, 44. ISSN: 1538-3881. <https://iopscience.iop.org/article/10.3847/0004-6256/151/2/44> (2021) (Feb. 2016).
17. Jones, D. H., Read, M. A., Saunders, W., *et al.* The 6dF Galaxy Survey: final redshift release (DR3) and southern large-scale structures. en. *Monthly Notices of the Royal Astronomical Society* **399**, 683–698. ISSN: 00358711, 13652966. <https://academic.oup.com/mnras/article-lookup/doi/10.1111/j.1365-2966.2009.15338.x> (2021) (Oct. 2009).
18. Parkinson, D., Riemer-Sørensen, S., Blake, C., *et al.* The WiggleZ Dark Energy Survey: Final data release and cosmological results. en. *Phys. Rev. D* **86**. arXiv: 1210.2130, 103518. ISSN: 1550-7998, 1550-2368. <http://arxiv.org/abs/1210.2130> (2021) (Nov. 2012).
19. Tegmark, M. Measuring Cosmological Parameters with Galaxy Surveys. en. *Phys. Rev. Lett.* **79**, 3806–3809. ISSN: 0031-9007, 1079-7114. <https://link.aps.org/doi/10.1103/PhysRevLett.79.3806> (2021) (Nov. 1997).
20. White, M., Song, Y.-S. & Percival, W. J. Forecasting Cosmological Constraints from Redshift Surveys. en. *Monthly Notices of the Royal Astronomical Society* **397**. arXiv: 0810.1518, 1348–1354. ISSN: 00358711, 13652966. <http://arxiv.org/abs/0810.1518> (2020) (Aug. 2009).
21. Font-Ribera, A., McDonald, P., Mostek, N., Reid, B. A., Seo, H.-J. & Slosar, A. DESI and other dark energy experiments in the era of neutrino mass measurements. en. *J. Cosmol. Astropart. Phys.* **2014**. arXiv: 1308.4164, 023–023. ISSN: 1475-7516. <http://arxiv.org/abs/1308.4164> (2021) (May 2014).
22. Zhao, G.-B., Wang, Y., Ross, A. J., *et al.* The extended Baryon Oscillation Spectroscopic Survey (eBOSS): a cosmological forecast. en. *arXiv:1510.08216 [astro-ph]*. arXiv: 1510.08216. <http://arxiv.org/abs/1510.08216> (2020) (Feb. 2016).
23. Fisher, R. A. The Logic of Inductive Inference. *Journal of the Royal Statistical Society* **98**. Publisher: [Wiley, Royal Statistical Society], 39–82. ISSN: 0952-8385. <https://www.jstor.org/stable/2342435> (2021) (1935).

24. Ruggeri, R. & Blake, C. How accurately can we measure the baryon acoustic oscillation feature? en. *Monthly Notices of the Royal Astronomical Society* **498**. arXiv: 1909.13011, 3744–3757. ISSN: 0035-8711, 1365-2966. <http://arxiv.org/abs/1909.13011> (2021) (Sept. 2020).
25. Tegmark, M., Taylor, A. & Heavens, A. Karhunen-Loeve eigenvalue problems in cosmology: how should we tackle large data sets? en. *ApJ* **480**. arXiv: astro-ph/9603021, 22–35. ISSN: 0004-637X, 1538-4357. <http://arxiv.org/abs/astro-ph/9603021> (2020) (May 1997).
26. Seo, H.-J. & Eisenstein, D. J. Improved forecasts for the baryon acoustic oscillations and cosmological distance scale. en. *ApJ* **665**. arXiv: astro-ph/0701079, 14–24. ISSN: 0004-637X, 1538-4357. <http://arxiv.org/abs/astro-ph/0701079> (2020) (Aug. 2007).
27. Eisenstein, D. J. & Hu, W. Baryonic Features in the Matter Transfer Function. en. *ApJ* **496**, 605–614. ISSN: 0004-637X, 1538-4357. <https://iopscience.iop.org/article/10.1086/305424> (2020) (Apr. 1998).
28. Peebles, P. J. E. Tracing galaxy orbits back in time. en. *ApJ* **344**, L53. ISSN: 0004-637X, 1538-4357. <http://adsabs.harvard.edu/doi/10.1086/185529> (2021) (Sept. 1989).
29. Eisenstein, D. J., Seo, H.-J., Sirko, E. & Spergel, D. N. Improving Cosmological Distance Measurements by Reconstruction of the Baryon Acoustic Peak. en. *ApJ* **664**, 675–679. ISSN: 0004-637X, 1538-4357. <https://iopscience.iop.org/article/10.1086/518712> (2021) (Aug. 2007).
30. Beutler, F., Seo, H.-J., Saito, S., *et al.* The clustering of galaxies in the completed SDSS-III Baryon Oscillation Spectroscopic Survey: anisotropic galaxy clustering in Fourier space. en. *Mon. Not. R. Astron. Soc.* **466**, 2242–2260. ISSN: 0035-8711, 1365-2966. <https://academic.oup.com/mnras/article-lookup/doi/10.1093/mnras/stw3298> (2021) (Apr. 2017).
31. Okumura, T., Seljak, U., McDonald, P. & Desjacques, V. Distribution function approach to redshift space distortions. Part II: N-body simulations. en. *arXiv:1109.1609 [astro-ph]*. arXiv: 1109.1609. <http://arxiv.org/abs/1109.1609> (2021) (Feb. 2012).
32. Zarrouk, P., Burtin, E., Gil-Marin, H., *et al.* The clustering of the SDSS-IV extended Baryon Oscillation Spectroscopic Survey DR14 quasar sample: measurement of the growth rate of structure from the anisotropic correlation function between redshift 0.8 and 2.2. en. *Monthly Notices of the Royal Astronomical Society* **477**. arXiv: 1801.03062, 1639–1663. ISSN: 0035-8711, 1365-2966. <http://arxiv.org/abs/1801.03062> (2021) (June 2018).
33. Eisenstein, D. J., Seo, H.-j. & White, M. On the Robustness of the Acoustic Scale in the Low-Redshift Clustering of Matter. en. *ApJ* **664**. arXiv: astro-ph/0604361, 660–674. ISSN: 0004-637X, 1538-4357. <http://arxiv.org/abs/astro-ph/0604361> (2020) (Aug. 2007).
34. Padmanabhan, N., White, M. & Cohn, J. D. Reconstructing baryon oscillations: A Lagrangian theory perspective. en. *Phys. Rev. D* **79**, 063523. ISSN: 1550-7998, 1550-2368. <https://link.aps.org/doi/10.1103/PhysRevD.79.063523> (2021) (Mar. 2009).

35. Burden, A., Percival, W. J., Manera, M., Cuesta, A. J., Magana, M. V. & Ho, S. Efficient Reconstruction of Linear Baryon Acoustic Oscillations in Galaxy Surveys. en. *Monthly Notices of the Royal Astronomical Society* **445**. arXiv: 1408.1348, 3152–3168. ISSN: 1365-2966, 0035-8711. <http://arxiv.org/abs/1408.1348> (2021) (Dec. 2014).
36. Burden, A., Percival, W. J. & Howlett, C. Reconstruction in Fourier space. en. *Mon. Not. R. Astron. Soc.* **453**, 456–468. ISSN: 0035-8711, 1365-2966. <https://academic.oup.com/mnras/article-lookup/doi/10.1093/mnras/stv1581> (2021) (Oct. 2015).
37. Padmanabhan, N., Xu, X., Eisenstein, D. J., Scalzo, R., Cuesta, A. J., Mehta, K. T. & Kazin, E. A 2 per cent distance to $z = 0.35$ by reconstructing baryon acoustic oscillations – I. Methods and application to the Sloan Digital Sky Survey: A 2 per cent distance to $z = 0.35$. en. *Monthly Notices of the Royal Astronomical Society* **427**, 2132–2145. ISSN: 00358711, 13652966. <https://academic.oup.com/mnras/article-lookup/doi/10.1111/j.1365-2966.2012.21888.x> (2021) (Dec. 2012).
38. Birkin, J., Li, B., Cautun, M. & Shi, Y. Reconstructing the baryon acoustic oscillations using biased tracers. en. *Monthly Notices of the Royal Astronomical Society* **483**. arXiv: 1809.08135, 5267–5280. ISSN: 0035-8711, 1365-2966. <http://arxiv.org/abs/1809.08135> (2021) (Mar. 2019).
39. Sarpa, E., Schimd, C., Branchini, E. & Matarrese, S. BAO reconstruction: a swift numerical action method for massive spectroscopic surveys. en. *Monthly Notices of the Royal Astronomical Society* **484**. arXiv: 1809.10738, 3818–3830. ISSN: 0035-8711, 1365-2966. <http://arxiv.org/abs/1809.10738> (2021) (Apr. 2019).
40. Modi, C., Feng, Y. & Seljak, U. Cosmological Reconstruction From Galaxy Light: Neural Network Based Light-Matter Connection. en. *J. Cosmol. Astropart. Phys.* **2018**. arXiv: 1805.02247, 028–028. ISSN: 1475-7516. <http://arxiv.org/abs/1805.02247> (2021) (Oct. 2018).
41. Nikakhtar, F., Sheth, R. K. & Zehavi, I. Laguerre reconstruction of the correlation function on Baryon Acoustic Oscillation scales. en. *arXiv:2101.08376 [astro-ph]*. arXiv: 2101.08376. <http://arxiv.org/abs/2101.08376> (2021) (Jan. 2021).
42. Kaiser, N. Clustering in real space and in redshift space. *Monthly Notices of the Royal Astronomical Society* **227**, 1–21. ISSN: 0035-8711. <https://doi.org/10.1093/mnras/227.1.1> (2021) (July 1987).
43. Scoccimarro, R. Redshift-Space Distortions, Pairwise Velocities and Nonlinearities. en. *Phys. Rev. D* **70**. arXiv: astro-ph/0407214, 083007. ISSN: 1550-7998, 1550-2368. <http://arxiv.org/abs/astro-ph/0407214> (2021) (Oct. 2004).
44. Taruya, A., Nishimichi, T. & Saito, S. Baryon acoustic oscillations in 2D: Modeling redshift-space power spectrum from perturbation theory. en. *Phys. Rev. D* **82**, 063522. ISSN: 1550-7998, 1550-2368. <https://link.aps.org/doi/10.1103/PhysRevD.82.063522> (2021) (Sept. 2010).
45. Reid, B. A. & White, M. Towards an accurate model of the redshiftspace clustering of haloes in the quasilinear regime. en, 15 (2011).
46. Wang, L., Reid, B. & White, M. An analytic model for redshift-space distortions. en. *Monthly Notices of the Royal Astronomical Society* **437**, 588–599. ISSN: 0035-8711, 1365-2966. <http://academic.oup.com/mnras/article/437/1/588/1006043/An-analytic-model-for-redshiftspace-distortions> (2021) (Jan. 2014).

47. Jennings, E., Baugh, C. M. & Pascoli, S. Modelling redshift space distortions in hierarchical cosmologies: Redshift space distortions. en. *Monthly Notices of the Royal Astronomical Society*, no–no. ISSN: 00358711. <https://academic.oup.com/mnras/article-lookup/doi/10.1111/j.1365-2966.2010.17581.x> (2021) (Oct. 2010).
48. Sánchez, A. G., Kazin, E. A., Beutler, F., *et al.* The clustering of galaxies in the SDSS-III Baryon Oscillation Spectroscopic Survey: cosmological constraints from the full shape of the clustering wedges. en. *Monthly Notices of the Royal Astronomical Society* **433**, 1202–1222. ISSN: 1365-2966, 0035-8711. <http://academic.oup.com/mnras/article/433/2/1202/1748526/The-clustering-of-galaxies-in-the-SDSSIII-Baryon> (2021) (Aug. 2013).
49. Crocce, M. & Scoccimarro, R. Renormalized Cosmological Perturbation Theory. en. *Phys. Rev. D* **73**. arXiv: astro-ph/0509418, 063519. ISSN: 1550-7998, 1550-2368. <http://arxiv.org/abs/astro-ph/0509418> (2021) (Mar. 2006).
50. Sánchez, A. G., Scoccimarro, R., Crocce, M., *et al.* The clustering of galaxies in the completed SDSS-III Baryon Oscillation Spectroscopic Survey: Cosmological implications of the configuration-space clustering wedges. en. *Mon. Not. R. Astron. Soc.* **464**, 1640–1658. ISSN: 0035-8711, 1365-2966. <https://academic.oup.com/mnras/article-lookup/doi/10.1093/mnras/stw2443> (2021) (Jan. 2017).
51. Pezzotta, A., Crocce, M., Eggemeier, A., Sánchez, A. G. & Scoccimarro, R. Testing one-loop galaxy bias: cosmological constraints from the power spectrum. *arXiv e-prints*, arXiv:2102.08315. arXiv: [2102.08315](https://arxiv.org/abs/2102.08315) [astro-ph.CO] (Feb. 2021).
52. Grieb, J. N., Sánchez, A. G., Salazar-Albornoz, S., *et al.* The clustering of galaxies in the completed SDSS-III Baryon Oscillation Spectroscopic Survey: Cosmological implications of the Fourier space wedges of the final sample. en. *Mon. Not. R. Astron. Soc.* arXiv: 1607.03143, stw3384. ISSN: 0035-8711, 1365-2966. <http://arxiv.org/abs/1607.03143> (2021) (Jan. 2017).
53. Jones, D. H., Saunders, W., Colless, M., *et al.* The 6dF Galaxy Survey: Samples, Observational Techniques and the First Data Release. en. *Monthly Notices of the Royal Astronomical Society* **355**. arXiv: astro-ph/0403501, 747–763. ISSN: 0035-8711, 1365-2966. <http://arxiv.org/abs/astro-ph/0403501> (2021) (Dec. 2004).
54. Carter, P., Beutler, F., Percival, W. J., Blake, C., Koda, J. & Ross, A. J. Low Redshift Baryon Acoustic Oscillation Measurement from the Reconstructed 6-degree Field Galaxy Survey. en. *Monthly Notices of the Royal Astronomical Society* **481**. arXiv: 1803.01746, 2371–2383. ISSN: 0035-8711, 1365-2966. <http://arxiv.org/abs/1803.01746> (2021) (Dec. 2018).
55. Beutler, F., Blake, C., Colless, M., *et al.* The 6dF Galaxy Survey: Baryon Acoustic Oscillations and the Local Hubble Constant. en. *Monthly Notices of the Royal Astronomical Society* **416**. arXiv: 1106.3366, 3017–3032. ISSN: 00358711. <http://arxiv.org/abs/1106.3366> (2020) (Oct. 2011).
56. Beutler, F., Blake, C., Colless, M., *et al.* The 6dF Galaxy Survey: $z \approx 0$ measurements of the growth rate and σ_8 : 6dFGS: $z \approx 0$ measurements of $f\sigma_8$ and σ_8 . en. *Monthly Notices of the Royal Astronomical Society* **423**, 3430–3444. ISSN: 00358711. <https://academic.oup.com/mnras/article-lookup/doi/10.1111/j.1365-2966.2012.21136.x> (2021) (July 2012).

57. Gunn, J. E., Siegmund, W. A., Mannery, E. J., *et al.* The 2.5 m Telescope of the Sloan Digital Sky Survey. en. *AJ* **131**, 2332–2359. ISSN: 0004-6256, 1538-3881. <https://iopscience.iop.org/article/10.1086/500975> (2021) (Apr. 2006).
58. Ross, A. J., Samushia, L., Howlett, C., Percival, W. J., Burden, A. & Manera, M. The Clustering of the SDSS DR7 Main Galaxy Sample I: A 4 per cent Distance Measure at $z=0.15$. en. *Monthly Notices of the Royal Astronomical Society* **449**. arXiv: 1409.3242, 835–847. ISSN: 1365-2966, 0035-8711. <http://arxiv.org/abs/1409.3242> (2020) (May 2015).
59. Howlett, C., Ross, A. J., Samushia, L., Percival, W. J. & Manera, M. The Clustering of the SDSS Main Galaxy Sample II: Mock galaxy catalogues and a measurement of the growth of structure from Redshift Space Distortions at $z=0.15$. en. *Monthly Notices of the Royal Astronomical Society* **449**. arXiv: 1409.3238, 848–866. ISSN: 1365-2966, 0035-8711. <http://arxiv.org/abs/1409.3238> (2020) (May 2015).
60. Reid, B., Ho, S., Padmanabhan, N., *et al.* SDSS-III Baryon Oscillation Spectroscopic Survey Data Release 12: galaxy target selection and large scale structure catalogues. en. *arXiv:1509.06529 [astro-ph]*. arXiv: 1509.06529. <http://arxiv.org/abs/1509.06529> (2021) (Oct. 2015).
61. Reid, B. A., Samushia, L., White, M., *et al.* The clustering of galaxies in the SDSS-III Baryon Oscillation Spectroscopic Survey: measurements of the growth of structure and expansion rate at $z=0.57$ from anisotropic clustering. en. *Monthly Notices of the Royal Astronomical Society* **426**. arXiv: 1203.6641, 2719–2737. ISSN: 00358711. <http://arxiv.org/abs/1203.6641> (2021) (Nov. 2012).
62. Anderson, L., Aubourg, E., Bailey, S., *et al.* The clustering of galaxies in the SDSS-III Baryon Oscillation Spectroscopic Survey: Baryon Acoustic Oscillations in the Data Release 10 and 11 galaxy samples. en. *Monthly Notices of the Royal Astronomical Society* **441**. arXiv: 1312.4877, 24–62. ISSN: 1365-2966, 0035-8711. <http://arxiv.org/abs/1312.4877> (2021) (June 2014).
63. Sánchez, A. G., Montesano, F., Kazin, E. A., *et al.* The clustering of galaxies in the SDSS-III Baryon Oscillation Spectroscopic Survey: cosmological implications of the full shape of the clustering wedges in the data release 10 and 11 galaxy samples. en. *Monthly Notices of the Royal Astronomical Society* **440**, 2692–2713. ISSN: 0035-8711, 1365-2966. <https://academic.oup.com/mnras/article/440/3/2692/1075640> (2021) (May 2014).
64. Samushia, L., Reid, B. A., White, M., *et al.* The Clustering of Galaxies in the SDSS-III Baryon Oscillation Spectroscopic Survey (BOSS): measuring growth rate and geometry with anisotropic clustering. en. *Monthly Notices of the Royal Astronomical Society* **439**. arXiv: 1312.4899, 3504–3519. ISSN: 1365-2966, 0035-8711. <http://arxiv.org/abs/1312.4899> (2021) (Apr. 2014).
65. Alam, S., Ata, M., Bailey, S., *et al.* The clustering of galaxies in the completed SDSS-III Baryon Oscillation Spectroscopic Survey: cosmological analysis of the DR12 galaxy sample. en. *Monthly Notices of the Royal Astronomical Society* **470**. arXiv: 1607.03155, 2617–2652. ISSN: 0035-8711, 1365-2966. <http://arxiv.org/abs/1607.03155> (2020) (Sept. 2017).

66. Gil-Marín, H., Percival, W. J., Cuesta, A. J., *et al.* The clustering of galaxies in the SDSS-III Baryon Oscillation Spectroscopic Survey: BAO measurement from the LOS-dependent power spectrum of DR12 BOSS galaxies. en. *Mon. Not. R. Astron. Soc.* **460**. arXiv: 1509.06373, 4210–4219. ISSN: 0035-8711, 1365-2966. <http://arxiv.org/abs/1509.06373> (2021) (Aug. 2016).
67. Zhao, C., Chuang, C.-H., Bautista, J., *et al.* The Completed SDSS-IV extended Baryon Oscillation Spectroscopic Survey: one thousand multi-tracer mock catalogues with redshift evolution and systematics for galaxies and quasars of the final data release. en. *arXiv:2007.08997 [astro-ph]*. arXiv: 2007.08997. <http://arxiv.org/abs/2007.08997> (2021) (July 2020).
68. Prakash, A., Licquia, T. C., Newman, J. A., *et al.* The SDSS-IV extended Baryonic Oscillation Spectroscopic Survey: Luminous Red Galaxy Target Selection. en. *ApJS* **224**. arXiv: 1508.04478, 34. ISSN: 1538-4365. <http://arxiv.org/abs/1508.04478> (2021) (June 2016).
69. Satpathy, S., Alam, S., Ho, S., *et al.* The clustering of galaxies in the completed SDSS-III Baryon Oscillation Spectroscopic Survey: On the measurement of growth rate using galaxy correlation functions. en. *Monthly Notices of the Royal Astronomical Society* **469**. arXiv: 1607.03148, 1369–1382. ISSN: 0035-8711, 1365-2966. <http://arxiv.org/abs/1607.03148> (2021) (Aug. 2017).
70. Gil-Marín, H., Percival, W. J., Cuesta, A. J., *et al.* The clustering of galaxies in the SDSS-III Baryon Oscillation Spectroscopic Survey: BAO measurement from the LOS-dependent power spectrum of DR12 BOSS galaxies. en. *Mon. Not. R. Astron. Soc.* **460**. arXiv: 1509.06373, 4210–4219. ISSN: 0035-8711, 1365-2966. <http://arxiv.org/abs/1509.06373> (2021) (Aug. 2016).
71. Ross, A. J., Bautista, J., Tojeiro, R., *et al.* The Completed SDSS-IV extended Baryon Oscillation Spectroscopic Survey: Large-scale Structure Catalogs for Cosmological Analysis. en. *Monthly Notices of the Royal Astronomical Society* **498**. arXiv: 2007.09000, 2354–2371. ISSN: 0035-8711, 1365-2966. <http://arxiv.org/abs/2007.09000> (2021) (Sept. 2020).
72. Raichoor, A., de Mattia, A., Ross, A. J., *et al.* The completed SDSS-IV extended Baryon Oscillation Spectroscopic Survey: Large-scale Structure Catalogues and Measurement of the isotropic BAO between redshift 0.6 and 1.1 for the Emission Line Galaxy Sample. en. *Monthly Notices of the Royal Astronomical Society* **500**. arXiv: 2007.09007, 3254–3274. ISSN: 0035-8711, 1365-2966. <http://arxiv.org/abs/2007.09007> (2021) (Dec. 2020).
73. Lyke, B. W., Higley, A. N., McLane, J. N., *et al.* The Sloan Digital Sky Survey Quasar Catalog: Sixteenth Data Release. en. *ApJS* **250**. arXiv: 2007.09001, 8. ISSN: 1538-4365. <http://arxiv.org/abs/2007.09001> (2021) (Aug. 2020).
74. Pâris, I., Petitjean, P., Aubourg, E., *et al.* The Sloan Digital Sky Survey Quasar Catalog: Fourteenth Data Release. en. *A&A* **613**. arXiv: 1712.05029, A51. ISSN: 0004-6361, 1432-0746. <http://arxiv.org/abs/1712.05029> (2021) (May 2018).

75. Bautista, J. E., Paviot, R., Magaña, M. V., *et al.* The Completed SDSS-IV extended Baryon Oscillation Spectroscopic Survey: measurement of the BAO and growth rate of structure of the luminous red galaxy sample from the anisotropic correlation function between redshifts 0.6 and 1. en. *Monthly Notices of the Royal Astronomical Society* **500**. arXiv: 2007.08993, 736–762. ISSN: 0035-8711, 1365-2966. <http://arxiv.org/abs/2007.08993> (2021) (Nov. 2020).
76. Gil-Marín, H., Bautista, J. E., Paviot, R., *et al.* The Completed SDSS-IV extended Baryon Oscillation Spectroscopic Survey: measurement of the BAO and growth rate of structure of the luminous red galaxy sample from the anisotropic power spectrum between redshifts 0.6 and 1.0. en. *Monthly Notices of the Royal Astronomical Society* **498**. arXiv: 2007.08994, 2492–2531. ISSN: 0035-8711, 1365-2966. <http://arxiv.org/abs/2007.08994> (2020) (Sept. 2020).
77. Bautista, J. E., Vargas-Magaña, M., Dawson, K. S., *et al.* The SDSS-IV Extended Baryon Oscillation Spectroscopic Survey: Baryon Acoustic Oscillations at Redshift of 0.72 with the DR14 Luminous Red Galaxy Sample. en. *ApJ* **863**, 110. ISSN: 1538-4357. <https://iopscience.iop.org/article/10.3847/1538-4357/aacea5> (2021) (Aug. 2018).
78. Icaza-Lizaola, M., Vargas-Magaña, M., Fromenteau, S., *et al.* The clustering of the SDSS-IV extended Baryon Oscillation Spectroscopic Survey DR14 LRG sample: structure growth rate measurement from the anisotropic LRG correlation function in the redshift range $0.6 < z < 1.0$. en. *Monthly Notices of the Royal Astronomical Society* **492**. arXiv: 1909.07742, 4189–4215. ISSN: 0035-8711, 1365-2966. <http://arxiv.org/abs/1909.07742> (2021) (Mar. 2020).
79. De Mattia, A., Ruhlmann-Kleider, V., Raichoor, A., *et al.* The Completed SDSS-IV extended Baryon Oscillation Spectroscopic Survey: measurement of the BAO and growth rate of structure of the emission line galaxy sample from the anisotropic power spectrum between redshift 0.6 and 1.1. en. *arXiv:2007.09008 [astro-ph]*. arXiv: 2007.09008. <http://arxiv.org/abs/2007.09008> (2020) (July 2020).
80. Tamone, A., Raichoor, A., Zhao, C., *et al.* The Completed SDSS-IV extended Baryon Oscillation Spectroscopic Survey: Growth rate of structure measurement from anisotropic clustering analysis in configuration space between redshift 0.6 and 1.1 for the Emission Line Galaxy sample. en. *Monthly Notices of the Royal Astronomical Society* **499**. arXiv: 2007.09009, 5527–5546. ISSN: 0035-8711, 1365-2966. <http://arxiv.org/abs/2007.09009> (2021) (Nov. 2020).
81. Neveux, R., Burtin, E., de Mattia, A., *et al.* The Completed SDSS-IV extended Baryon Oscillation Spectroscopic Survey: BAO and RSD measurements from the anisotropic power spectrum of the Quasar sample between redshift 0.8 and 2.2. en. *arXiv:2007.08999 [astro-ph]*. arXiv: 2007.08999. <http://arxiv.org/abs/2007.08999> (2020) (July 2020).
82. Croom, S. M., Boyle, B. J., Shanks, T., *et al.* The 2dF QSO Redshift Survey - XIV. Structure and evolution from the two-point correlation function. en. *Monthly Notices of the Royal Astronomical Society* **356**, 415–438. ISSN: 00358711, 13652966. <https://academic.oup.com/mnras/article-lookup/doi/10.1111/j.1365-2966.2004.08379.x> (2021) (Jan. 2005).

83. Hou, J., Sánchez, A. G., Ross, A. J., *et al.* The Completed SDSS-IV extended Baryon Oscillation Spectroscopic Survey: BAO and RSD measurements from anisotropic clustering analysis of the Quasar Sample in configuration space between redshift 0.8 and 2.2. en. *arXiv:2007.08998 [astro-ph]*. arXiv: 2007.08998. <http://arxiv.org/abs/2007.08998> (2020) (July 2020).
84. Ata, M., Baumgarten, F., Bautista, J., *et al.* The clustering of the SDSS-IV extended Baryon Oscillation Spectroscopic Survey DR14 quasar sample: First measurement of Baryon Acoustic Oscillations between redshift 0.8 and 2.2. en. *Monthly Notices of the Royal Astronomical Society* **473**. arXiv: 1705.06373, 4773–4794. ISSN: 0035-8711, 1365-2966. <http://arxiv.org/abs/1705.06373> (2021) (Feb. 2018).
85. Drinkwater, M. J., Jurek, R. J., Blake, C., *et al.* The WiggleZ Dark Energy Survey: Survey Design and First Data Release. en. *Monthly Notices of the Royal Astronomical Society* **401**. arXiv: 0911.4246, 1429–1452. ISSN: 00358711, 13652966. <http://arxiv.org/abs/0911.4246> (2021) (Jan. 2010).
86. Blake, C., Brough, S., Colless, M., *et al.* The WiggleZ Dark Energy Survey: Joint measurements of the expansion and growth history at $z < 1$. en. *Monthly Notices of the Royal Astronomical Society* **425**. arXiv: 1204.3674, 405–414. ISSN: 00358711. <http://arxiv.org/abs/1204.3674> (2020) (Sept. 2012).
87. Kazin, E. A., Koda, J., Blake, C., *et al.* The WiggleZ Dark Energy Survey: Improved Distance Measurements to $z = 1$ with Reconstruction of the Baryonic Acoustic Feature. en. *Monthly Notices of the Royal Astronomical Society* **441**. arXiv: 1401.0358, 3524–3542. ISSN: 1365-2966, 0035-8711. <http://arxiv.org/abs/1401.0358> (2020) (July 2014).
88. Feldman, H. A., Kaiser, N. & Peacock, J. A. Power Spectrum Analysis of Three-Dimensional Redshift Surveys. en. *ApJ* **426**. arXiv: astro-ph/9304022, 23. ISSN: 0004-637X, 1538-4357. <http://arxiv.org/abs/astro-ph/9304022> (2021) (May 1994).
89. Carrasco, J. J. M., Hertzberg, M. P. & Senatore, L. The effective field theory of cosmological large scale structures. en. *J. High Energ. Phys.* **2012**, 82. ISSN: 1029-8479. [http://link.springer.com/10.1007/JHEP09\(2012\)082](http://link.springer.com/10.1007/JHEP09(2012)082) (2021) (Sept. 2012).
90. Baumann, D., Nicolis, A., Senatore, L. & Zaldarriaga, M. Cosmological non-linearities as an effective fluid. en. *J. Cosmol. Astropart. Phys.* **2012**, 051–051. ISSN: 1475-7516. <https://iopscience.iop.org/article/10.1088/1475-7516/2012/07/051> (2021) (July 2012).
91. Ivanov, M. M., McDonough, E., Hill, J. C., Simonović, M., Toomey, M. W., Alexander, S. & Zaldarriaga, M. Constraining Early Dark Energy with Large-Scale Structure. en. *Phys. Rev. D* **102**. arXiv: 2006.11235, 103502. ISSN: 2470-0010, 2470-0029. <http://arxiv.org/abs/2006.11235> (2021) (Nov. 2020).
92. D’Amico, G., Gleyzes, J., Kokron, N., Markovic, D., Senatore, L., Zhang, P., Beutler, F. & Gil-Marín, H. The Cosmological Analysis of the SDSS/BOSS data from the Effective Field Theory of Large-Scale Structure. en. *J. Cosmol. Astropart. Phys.* **2020**. arXiv: 1909.05271, 005–005. ISSN: 1475-7516. <http://arxiv.org/abs/1909.05271> (2021) (May 2020).

93. Chen, S.-F., Vlah, Z., Castorina, E. & White, M. Redshift-space distortions in Lagrangian perturbation theory. en. *J. Cosmol. Astropart. Phys.* **2021**, 100. ISSN: 1475-7516. <https://iopscience.iop.org/article/10.1088/1475-7516/2021/03/100> (2021) (Mar. 2021).
94. Kokron, N., DeRose, J., Chen, S.-F., White, M. & Wechsler, R. H. The cosmology dependence of galaxy clustering and lensing from a hybrid N -body-perturbation theory model. en. *arXiv:2101.11014 [astro-ph]*. arXiv: 2101.11014. <http://arxiv.org/abs/2101.11014> (2021) (Jan. 2021).
95. Zhai, Z., Tinker, J. L., Becker, M. R., *et al.* The Aemulus Project. III. Emulation of the Galaxy Correlation Function. en. *ApJ* **874**, 95. ISSN: 1538-4357. <https://iopscience.iop.org/article/10.3847/1538-4357/ab0d7b> (2021) (Mar. 2019).
96. Reid, B. A., Seo, H.-J., Leauthaud, A., Tinker, J. L. & White, M. A 2.5% measurement of the growth rate from small-scale redshift space clustering of SDSS-III CMASS galaxies. en. *Monthly Notices of the Royal Astronomical Society* **444**. arXiv: 1404.3742, 476–502. ISSN: 0035-8711, 1365-2966. <http://arxiv.org/abs/1404.3742> (2021) (Oct. 2014).
97. Lange, J. U., Hearin, A. P., Leauthaud, A., Bosch, F. C. v. d., Guo, H. & DeRose, J. Five-percent measurements of the growth rate from simulation-based modelling of redshift-space clustering in BOSS LOWZ. en. *arXiv:2101.12261 [astro-ph]*. arXiv: 2101.12261. <http://arxiv.org/abs/2101.12261> (2021) (Jan. 2021).
98. DeRose, J., Becker, M. R. & Wechsler, R. H. Modeling Redshift-Space Clustering with Abundance Matching. *arXiv e-prints*, arXiv:2105.12104. arXiv: [2105.12104](https://arxiv.org/abs/2105.12104) [[astro-ph.CO](https://arxiv.org/abs/2105.12104)] (May 2021).
99. Kobayashi, Y., Nishimichi, T., Takada, M., Takahashi, R. & Osato, K. Accurate emulator for the redshift-space power spectrum of dark matter halos and its application to galaxy power spectrum. en. *Phys. Rev. D* **102**. arXiv: 2005.06122, 063504. ISSN: 2470-0010, 2470-0029. <http://arxiv.org/abs/2005.06122> (2021) (Sept. 2020).
100. Van der Walt, S., Colbert, S. C. & Varoquaux, G. The NumPy Array: A Structure for Efficient Numerical Computation. *Computing in Science Engineering* **13**, 22–30 (2011).
101. Virtanen, P., Gommers, R., Oliphant, T. E., *et al.* SciPy 1.0: Fundamental Algorithms for Scientific Computing in Python. *Nature Methods* **17**, 261–272 (2020).
102. Hunter, J. D. Matplotlib: A 2D Graphics Environment. *Computing in Science Engineering* **9**, 90–95 (2007).
103. Diemer, B. COLOSSUS: A Python Toolkit for Cosmology, Large-scale Structure, and Dark Matter Halos. en. *ApJS* **239**, 35. ISSN: 1538-4365. <https://iopscience.iop.org/article/10.3847/1538-4365/aeee8c> (2021) (Dec. 2018).
104. The Astropy Collaboration, Robitaille, Thomas P., Tollerud, Erik J., *et al.* Astropy: A community Python package for astronomy. *A&A* **558**, A33. <https://doi.org/10.1051/0004-6361/201322068> (2013).
105. Samushia, L., Percival, W. J., Guzzo, L., *et al.* Effects of cosmological model assumptions on galaxy redshift survey measurements. en. *Monthly Notices of the Royal Astronomical Society*. arXiv: 1006.0609, no–no. ISSN: 00358711. <http://arxiv.org/abs/1006.0609> (2021) (Oct. 2010).